Bidirectional GABAergic control of AP firing in newly-generated young granule cells of the adult hippocampus

Inauguraldissertation

zur

Erlangung der Würde eines Doktors der Philosophie

vorgelegt der

Philosophisch-Naturwissenschaftlichen Fakultät

der Universität Basel

von

Stefanie Heigele

aus Ulm, Deutschland

Basel, 2015

Genehmigt von der Philosophisch-Naturwissenschaftlichen Fakultät auf Antrag von

Prof. Dr. Josef Bischofberger

Fakultätsverantwortlicher und Dissertationsleiter

Prof. Dr. Sonja Hofer

Korreferentin

Basel, den 21. April 2015

Prof. Dr. Jörg Schibler

Dekan

Contents

1 Abstract

Gamma-aminobutyric acid (GABA) is the first transmitter which provides synaptic input to newly generated neurons. In the first 2-3 weeks after mitosis, young neurons show an elevated intracellular chloride concentration due to the expression of the NKCC1 Cl^--importer. Hence, GABAergic transmission provides depolarization to the newborn cells, which is known to be crucial for activity-dependent cell survival, development and functional maturation. However, it is still unknown whether activation of GABAergic synapses can evoke action potential (AP) firing in newly generated granule cells of the adult hippocampus to induce these trophic effects. In order to address this question, young neurons of the adult brain were fluorescently labeled using either retrovirus-based GFP expression or transgenic mice expressing the red fluorescent protein DsRed under the control of the doublecortin (DCX)-promoter. Electrophysiological recordings were performed on acute hippocampal brain slices. Gramicidin perforated-patch recordings revealed a reversal potential of GABAergic synaptic currents substantially more positive in 2-3 week old DCX-expressing neurons (~-35 mV) as compared to mature granule cells (~-75 mV). In both perforated-patch and whole-cell configuration, GABAergic synaptic currents are indeed able to excite AP firing and to modulate glutamatergic subthreshold inputs. Due to the high input resistance and the slow membrane time constant of young granule cells, low GABAergic synaptic inputs result in a long lasting depolarization, which provides the basis for an efficient temporal integration of excitatory postsynaptic potentials with an enhanced firing probability for ~200 ms. Thereby, GABAergic synaptic currents boost AP firing in young granule cells within a conductance window between ~0.5 and 3.5 nS. Larger GABAergic inputs however effectively block AP firing via shunting inhibition, which might be important to protect the young cells from over excitation. Synaptic GABAergic transmission was fully blocked by 10 µM gabazine, whereas a half maximal inhibitory concentration (0.2 µM) increased AP firing at high stimulation intensities, showing that both AP generation and shunting inhibition are mediated by $GABA_A$ receptor mediated chloride conductances. Taken together, this study shows that GABAergic synaptic inputs in newly generated young granule cells can dynamically support either AP firing or shunting inhibition dependent on hippocampal network activity.

2 Introduction

2.1 Neurogenesis in the adult brain

The dynamic growth of the developing brain during embryogenesis is in stark contrast to the relative stability after birth. For a long time it was believed that the number of neurons stayed fixed from soon after birth and early leading scientists like Ramón y Cajal concluded that neurogenesis does not take place in the adult brain. In the 1960s, the discovery of adult neurogenesis overturned this long-held dogma (Altman 1962). Altman and colleagues demonstrated the existence of newly generated neurons in the postnatal mammalian brain by autoradiographical studies on thymidine-H(3) injected rats, which is incorporated into the DNA and thereby labels dividing cells (Altman 1963, Altman & Das 1965). It is now generally accepted that there are two discrete regions in the mammalian brain where newborn neurons can be generated from neural progenitor cells throughout life. Neurons born in the subventricular zone (SVZ) that lines the walls of the lateral ventricle migrate along the rostral migratory stream to the olfactory bulb where they differentiate into multiple types of local circuit interneurons (Doetsch et al. 1999, Mirzadeh et al. 2008, Fuentealba et al. 2012). Neurons born in the subgranular zone of the dentate gyrus mature into glutamatergic granule cells and integrate into the local network (Kaplan and Hinds, 1977). Other neurogenic regions like the neocortex of adult rodents are sporadically suggested, but this has remained controversial so far (Kaplan 1981, Magavi et al. 2000).

In the last decades, several studies demonstrated post-developmental neurogenesis in different species including songbirds (Nottebohm et al. 1981, Alvarez-Buylla and Nottebohm 1988), rodents (Kaplan 1981, Kempermann 1997), marsupials (Harman et al. 2003, Grabiec et al. 2009), and primates (Gould et al. 1999, Kornack and Rakic 1999). Although SVZ adult neurogenesis in humans is still a matter of debate (Wang et al. 2011, Bergmann et al. 2012, Ernst et al. 2014), several studies revealed profound neurogenesis in the human dentate gyrus, partially from investigations on cancer patients with DNA-incorporating agents (Eriksson et al. 1998, 2011, Maguire et al. 2000). A recent study assessed the generation of hippocampal granule cells using a novel approach of carbon dating. Spalding et al. (2013) measured the concentration of nuclear-bomb-test derived ^{14}C in genomic DNA. Although no evidence of ongoing

neurogenesis was detected in the olfactory bulb, they could show that in adult humans on average approximately 700 new neurons were added in each hippocampus per day.

The hippocampal formation is essential for our conscious memory of facts and events (Scoville and Milner 1957, Squire et al. 2004). Furthermore, it contributes to the spatial orientation in a given environment (O'Keefe and Dostrovsky 1971, O´Keefe 1976, Leutgeb et al. 2007). In addition to the known synaptic plasticity, the continuous generation and integration of new neurons throughout the life of an animal provides an important mechanism of structural plasticity. During the physiological ageing process, a decline of cognitive skills can be observed which is accompanied by a decline in the rate of hippocampal neurogenesis (Kuhn et al. 1996, Kempermann et al. 1998, Bizon and Gallagher 2003, Ben Abdallah et al. 2010). Pathological alterations in adult neurogenesis could be linked to several neuro-degenerative and neuro-psychiatric diseases, like Alzheimer's disease, schizophrenia, epilepsy, anxiety or depression (Malberg et al. 2000, Namba et al. 2011, Jafari et al. 2012, Kheirbek et al. 2012, Wang et al. 2014). Further investigations of the physiological processes regulating adult neurogenesis may help to provide a better understanding of the causal relationships to misregulation in pathology.

2.2 Labeling techniques of newly generated neurons

Comprehensive research was performed investigating newly generated granule cells in the rodent hippocampus following the invention of several new methodologies (Lledo et al. 2006, Drew et al. 2013).

Bromodeoxyuridine (BrdU) is a thymidine analog that incorporates into the DNA during mitosis and thereby labels dividing cells. Applied intraperitoneally, BrdU labels dividing cells for about two days (Takahashi et al. 1992). After a certain period of time, the brain tissue can be immunohistochemically analyzed and neurons with a known cell age can be identified (e.g. Kuhn et al. 1996, Cameron and McKay 2001). Several marker proteins like the polysialylated-neural cell adhesion molecule (PSA-NCAM) or DCX selectively expressed by immature neurons can be used for post-hoc analysis (Seki and Arai 1995, Snyder et al. 2009). Despite its usefulness, BrdU is not an ideal marker for neurogenesis as it incorporates also non-specifically into damaged cells

during cell repair, it is potentially toxic and provides limitations to histological analyses (Kuhn and Copper-Kuhn 2007).

A major breakthrough was the development of techniques that allow the visualization of individual newborn neurons in the living brain tissue. One technique uses retroviruses carrying transgenes for fluorescent proteins that selectively incorporate into the DNA of dividing progenitor cells (van Praag et al. 2002). These viruses can be injected into the dentate gyrus where they locally label neurons that are generated during a short time thereafter and hence are “birth-dated”. Subsequent recordings of electrophysiological properties from fluorescently labeled cells can correlate functional data with a precise cell age (Esposito et al. 2005, Ge et al. 2007b).

The regional restriction for cell labeling obtained by viral infections can be overcome with transgenic mice. For this, fluorescent protein sequences are stably integrated into the mouse genome and expressed throughout life. The expression of the fluorescent proteins is thereby regulated by promoters specific to certain cell types or phases of cell development. Overstreet et al. (2004) used proopiomelanocortin-enhanced green fluorescent protein (POMC-eGFP) mice to mark cells up to ~2 weeks of age. Couillard-Despres et al. (2006) used a transgenic mouse model where Discosoma sp. reef coral red fluorescent protein (DsRed) is expressed under the control of the doublecortin (DCX) promoter to label cells from one day to 3 weeks after birth (Cooper-Kuhn and Kuhn 2002, Brown et al. 2003). These genetically modified animals allow the investigation of electrophysiological properties of cell populations with similar developmental stage.

2.3 Adult neurogenesis in the dentate gyrus

Most hippocampal granule cells (GCs) are generated postnatally (Lledo et al. 2006). During early developmental and adult neurogenesis, newly generated neurons supplement the existing GC population rather than replacing mature neurons. Therefore, the total number of dentate GC increases over the life span in rodents (Bayer 1985, Boss et al. 1985, Crespo et al. 1986). The number of newly generated granule cells varies considerably across species. Dentate gyri of mice contain a total number of about 300,000 granule cells, with 200 new neurons added per day (Kempermann et al. 1997). In young adult rats, the neurogenic rate is approximately 3 times higher. Roughly 4,500 new neurons are being produced per day to the total

population of 2.4 million GCs (West et al. 1991, Cameron and McKay 2001). However, the majority of newborn GCs die before they are integrated into the dentate gyrus circuitry (Kempermann et al. 1997a, Biebl et al. 2000, Kempermann and Gage 2002b, Zhao et al. 2010). The number of surviving GCs rapidly declines after cell division and stabilizes at around 4 weeks after mitosis (Kempermann et al. 2003). Finally, approximately 6% of the granule cell population is younger than one month (Cameron & McKay 2001).

The newly generated granule cells run through a period of structural and functional maturation, which lasts for approximately 6 to 8 weeks. At the end, they are indistinguishable from mature GCs and fully integrated into the hippocampal network (Laplagne et al. 2006, Overstreet-Wadiche and Westbrook 2006, Piatti et al. 2011). Figure 1 summarizes the major changes of cellular, immunocytochemical and electrophysiological properties during granule cell maturation.

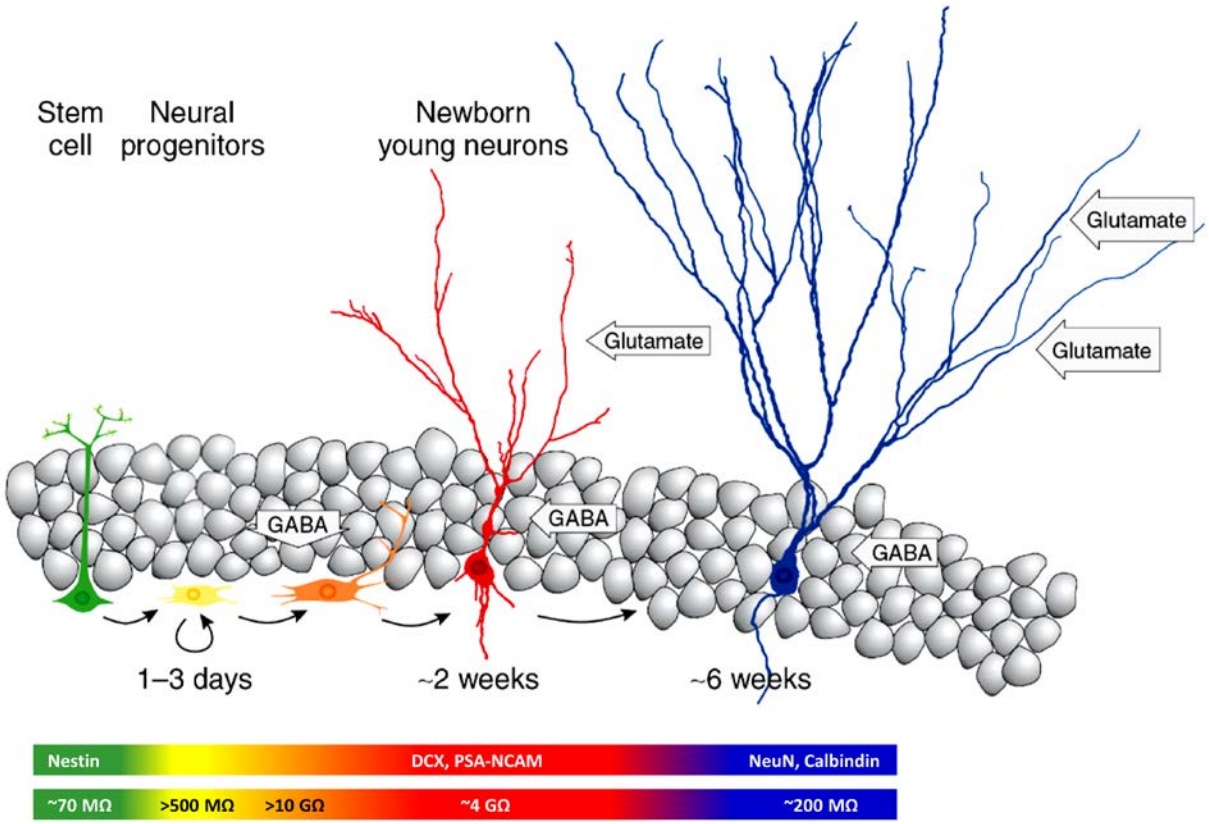

Figure 1 **Development of newly generated granule cells in the adult hippocampus.** Scheme depicting morphology, marker gene expression and input resistance of subsequent developmental stages. GABA is the first transmitter acting on newly generated neurons. Modified from Bischofberger (2007).

Newborn granule cells are generated from neural progenitor cells that are located in the subgranular zone (SGZ) at the inner border of the granule cell layer (GCL) next to the hilus. The SGZ neural progenitors express marker proteins like the glial fibrillary acidic protein (GFAP) and Nestin and can be divided into two subpopulations. The quiescent non-dividing radial glia cells have a thick dendrite which projects through the GCL into the inner molecular layer (ML) where it branches in short protrusions (Filippov et al. 2003, Fukuda et al. 2003). These cells are able to transform into active, dividing horizontal neural progenitor cells (Lugert et al. 2014). From *in vivo* clonal analysis it is known that the progenitors can either divide symmetrically in order to self-renew or divide asymmetrically to generate intermediate progenitor cells (Bonaguidi et al. 2011). The cell fate decision towards the neuronal lineage is made soon after cell division. These cells are then restricted to this lineage, exhibit an increased proliferative potential for about 3 days and finally differentiate into immature neurons, which migrate into the GCL. The local restriction of neural progenitor cells to the SGZ leads to a maturation gradient within the GCL with newborn young cells at the inner border close to the hilus and developmentally born mature cells close to the molecular layer (Crespo et al. 1986, Kempermann et al. 2003, Mathews et al. 2010).

The expression of DCX can be detected already one day after mitosis (Kempermann et al. 2003). DCX is a microtubule-associated protein which is involved in the rearrangement of actin filaments and hence primarily implicated in neuronal migration and neurite outgrowth (Francis et al. 1999, Gleeson et al. 1999, Tsukada et al. 2005). In the dentate gyrus it is reliably and selectively expressed in neuronal precursors and newborn cells (Brown et al. 2003, Rao and Shetty 2004, Couillard-Despres et al. 2005). During adult neurogenesis, the expression of DCX peaks during the first week, and is down-regulated concomitantly with the appearance of the mature neuronal marker NeuN within the next 2-3 weeks (Neuronal Nuclei, Mullen et al. 1992, Brown et al. 2003).

Immature granule cells have a small soma and a rudimentary dendritic tree (Ambrogini et al. 2004). According to the small cell size and low expression of voltage-independent potassium channels, the input resistance (R_{in}) of these cells is relatively high, up to several GΩ (Schmidt-Hieber et al. 2004, Mongiat et al. 2009, Schmidt-Salzmann et al. 2014). The adult-born GCs start very early to form afferent and efferent connections within the local neuronal network. During the first week after birth, the still

spineless dendrites grow into the molecular layer, where they receive first synaptic GABAergic inputs (Esposito et al. 2005, Wang et al. 2005, Ge et al. 2006, Markwardt et al. 2009). In contrast to the well-known inhibitory effect in mature neurons, young neurons are depolarized by GABAergic synaptic inputs (Figure 2a). Due to a high expression of the Na^+-K^+-$2Cl^-$ cotransporter (NKCC1), the intracellular Cl^- concentration is increased to about 25 mM (Esposito et al. 2005, Ge et al. 2006). As the ionotropic $GABA_A$ receptors mainly conduct chloride ions, GABAergic synaptic transmission results in Cl^- efflux and a depolarization from the resting membrane potential (Ben-Ari 2002, Ambrogini et al. 2004, Ge et al. 2006 Markwardt et al. 2008).

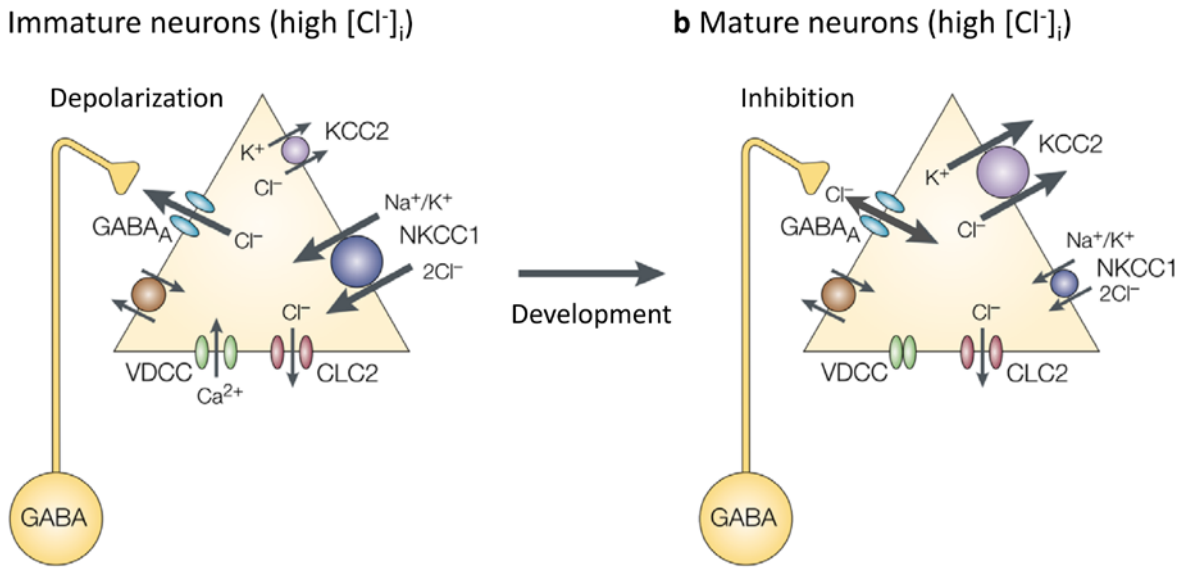

Figure 2 **Developmental change of intracellular chloride concentration is determined by NKCC1 and KCC2 expression levels.** Schematic diagram depicting the Na^+-K^+-$2Cl^-$ cotransporter (NKCC1), the K^+-Cl^- cotransporter (KCC2), voltage-gated calcium channels (VGCC) and voltage-gated chloride channel 2 (CLC2) as well as gradients for chloride ions. **a,** Early expression of NKCC1 results in an elevated intracellular chloride concentration ($[Cl^-]_i$) and a depolarizing GABA reversal potential (E_{GABA}). GABAergic transmission causes Cl^- efflux and depolarization of the cell. **b,** Expression of KCC2 predominates in mature neurons. Activity of Cl^- extruder reduces $[Cl^-]_i$ and hyperpolarizes E_{GABA} close to resting potential. GABAergic synaptic transmission induces shunting inhibition. Modified from Ben-Ari (2002).

During the second week after birth, the granule cell dendrites grow further into the molecular layer where they contact projections from the entorhinal cortex (perforant path) and hilar mossy cells. These fibers transmit glutamatergic synaptic input onto the first dendritic spines that are formed in the young neurons during the second week

(Zhao et al. 2006, Ge et al. 2006, Kumamoto et al. 2012, Vivar et al. 2012, Deshpande et al. 2013, Chancey et al. 2014). The glutamatergic inputs are initially small due to a low number of synapses (Esposito et al. 2005, Toni et al. 2007, Mongiat et al. 2009). At that time, the axons grow through the hilus and reach the CA3 region already at 12 days post mitosis (Stanfield and Trice 1988, Markakis and Gage 1999, Zhao et al. 2006). These mossy fibers form synapses onto GABAergic interneurons in the GCL, hilus, and CA3 as well as hilar mossy cells (Toni et al. 2008, Temprana et al. 2015). Large synaptic boutons on CA3 pyramidal cell dendrites were detected as early as 17 days after mitosis using three-dimensional reconstructions of synapses from electron micrographs (Toni et al. 2008). Gu et al. (2012) showed that these first anatomical connections are functional synapses, as they could record postsynaptic currents in CA3 pyramidal neurons elicited by adult-born dentate gyrus granule cells 2 weeks after mitosis.

During the third week after birth, several processes guide the cell to a mature state. The number of GABAergic and glutamatergic synaptic contacts increases rapidly, enlarging the amplitude of postsynaptic currents (Zhao et al. 2006, Toni and Sultan 2011). The input resistance continuously decreases due to an increased expression of K^+ leak channels (Liu et al. 1996, Schmidt-Hieber et al. 2004, Young et al. 2009). Finally, the GABA reversal potential (E_{GABA}) declines close to resting potential (Tozuka et al. 2005, Ge et al. 2006). The expression of NKCC1 is down-regulated accompanied by an up-regulated expression of the K^+-Cl^- extruder KCC2, resulting in a reduction of the intracellular Cl^- concentration (Figure 2b, Ganguly et al. 2001, Cancedda et al. 2007, Cellot and Cherubini 2013). Therefore, GABAergic synaptic transmission loses its depolarizing effect, but induces shunting inhibition by increasing the overall membrane conductance.

Around 4 weeks after birth, newborn young granule cells show already mature features including a large dendritic outgrowth, a high number of GABAergic and glutamatergic input synapses as well as profound output to CA3 pyramidal cells (van Praag et al. 2002, Esposito et al. 2005, Gu et al. 2012). The full development of inhibitory and excitatory synapses stabilizes after 6 to 8 weeks (Dieni et al. 2013).

The unique intrinsic properties make newly generated granule cells easily excitable. A high R_{in} and the expression of low-threshold transiently-activating T-type Ca^{2+}-channels enable the young neurons to fire action potentials (APs) in response to small

current injections (Schmidt-Hieber et al. 2004, Stocca et al. 2008, Schmidt-Salzmann et al. 2014). The high membrane time constant allows efficient temporal integration of postsynaptic potentials (Schmidt-Hieber et al. 2004, Stocca et al. 2008). Although excitatory postsynaptic inputs are still smaller than in mature neurons, the probability to fire APs in response to synaptic inputs is comparable in 3-4 week old GCs (Mongiat et al. 2009). The increased synaptic plasticity, as indicated by their lower threshold for the induction of long-term potentiation (LTP) and higher LTP amplitude (Schmidt-Hieber et al. 2004, Ge et al. 2007b, Bergami et al. 2015), make them suitable to participate in the information processing within the trisynaptic circuitry of the hippocampal formation (Aimone et al. 2010, Deng et al. 2010, Chancey et al. 2013, Cameron and Glover 2014).

2.4 Regulation of adult neurogenesis

Different intrinsic and extrinsic factors have been identified to regulate the extent of adult neurogenesis in the dentate gyrus. The most prominent enhancer of the neurogenic rate is an increased neuronal network activity in the dentate gyrus (Deissenroth et al. 2004). This can be achieved by physiological stimuli such as learning (Tronel et al. 2010), social interaction (Hsiao et al. 2014), physical exercise (van Praag et al. 1999, Zhao et al. 2006, Deshpande et al. 2013), or an enriched environment (Kempermann et al. 1997, Bergami et al. 2015). Interestingly, voluntary wheel running predominantly induces precursor cell proliferation, whereas a stimulating environment mainly promotes cell survival and therefore the number of GCs (Steiner et al. 2008, Fabel et al. 2009). Pathological enhancement of hippocampal activity as it occurs during epileptic seizures also stimulates granule cell proliferation and accelerates the integration of new granule cells, albeit a reduction of dendritic length can be observed (Parent et al. 1997, Parent and Lowenstein 2002, Overstreet-Wadiche et al. 2006). Stress (Gould et al. 1997) or the abuse of drugs or alcohol (Eisch et al. 2000, Vetreno and Crews 2015) have been shown to be negative regulators of adult neurogenesis. The rate of dentate gyrus neurogenesis also depends on the genetic background (Kempermann et al. 1997, Kempermann and Gage 2002, Snyder et al. 2009) and can be regulated for example by hormones such as steroids (Gould et al. 1992). A decline of adult neurogenesis can be observed during ageing. However, it is not yet completely understood why the neurogenic rate decreases with age, while

gliogenesis does not (Palmer et al. 2000, Seib et al. 2013). Possible mechanisms underlying this decrease include a decline in neurotrophic factors like neurotrophin-3 or brain-derived neurotrophic factor (BDNF) in the local environment (Kobilo et al. 2011, Marlatt et al. 2012, Bechara and Kelly 2013), age-related increase in glucocorticoids (Yagita et al. 2001), the intrinsic state of neural progenitor cells (Kuhn et al. 1996, Lugert et al. 2010) or the number of actively dividing progenitors (Bonaguidi et al. 2011).

2.5 GABAergic regulation of cell survival and maturation

Within the first 2 weeks, newborn granule cells go through a critical period where many cells die. Around 50-80% of adult-born GCs undergo programmed cell death (Cameron and McKay 2001, Dayer et al. 2003). What directs the selection of young neurons that remain to participate in the dentate gyrus network?

It could be shown that GABAergic and glutamatergic depolarization of embryonic cortical progenitor cells increase intracellular calcium levels and induce terminal differentiation into neurons (LoTurco et al. 1995). The calcium-dependent regulatory effect on neuronal differentiation of progenitors was subsequently reported also for the adult brain (Deisseroth et al. 2004, Tozuka et al. 2005). Interestingly, Tozuka et al. (2005) could show that in newly generated cells that do not yet receive glutamatergic inputs depolarization-mediated calcium influx initiates the expression of NeuroD. NeuroD is known to drive neuronal differentiation in hippocampal granule cells (Miyata et al. 1999, Liu et al. 2000). Furthermore, the administration of $GABA_A$-receptor agonists strongly increased the number of maturated neurons (Tozuka et al. 2005). These results indicate that $GABA_A$-dependent increase of intracellular calcium concentration is required for neuronal survival and differentiation of hippocampal precursor cells. The dependency of granule cell maturation on GABA-dependent depolarization was nicely shown by Ge et al. (2006). Using shRNA, the expression of NKCC1, the Cl^--importer essential for GABA-mediated depolarization in newborn young granule cells, was silenced. *Nkcc1*-shRNA-expressing newborn GCs miss the GABAergic depolarization and were shown to be delayed in terms of synaptic integration as well as dendritic outgrowth and branching. Similar results of GABA-dependent cell proliferation and dendritic maturation were recently shown for neural progenitors of the neonatal subventricular zone (Young et al. 2012). Therefore, GABA

does not only regulate survival and differentiation of newly generated granule cells but also synaptic and dendritic maturation.

In contrast to the trophic impact of GABA-dependent depolarization, GABA has been shown to act inhibitory on AP generation in postnatally born young granule cells. Overstreet-Wadiche et al. (2005) recorded from 1 to 2 week old proopiomelanocortin-(POMC) expressing cells. Bath-application of GABA blocked AP generation induced by current injection or spontaneous firing at more depolarized resting potential. Upon GABA-application, the cell membrane depolarized to the GABA reversal potential but sodium-mediated action potentials were prohibited, indicating that firing was blocked via shunting inhibition. However, whether synaptically transmitted GABA onto newly generated young granule cells induce AP firing or shunting inhibition has not yet been evaluated.

2.6 The aim of this work

In the present study, patch-clamp recordings in the perforated-patch and whole-cell configuration were used to explore $GABA_A$-mediated action potential firing in newborn hippocampal granule cells of the adult mouse brain. Four main questions were addressed in this study.

First, does synaptically transmitted GABA induce action potential firing or shunting inhibition?

Second, are GABAergic inputs able to modulate glutamatergic synaptic inputs? As the glutamatergic postsynaptic potentials are small in young neurons, they could be boosted by GABAergic depolarization to induce AP firing or shunting inhibition could efficiently prevent spiking.

Third, what are the requirements for action potential generation? In which way is action potential firing dependent on the strength of synaptic transmission and the relative timing of converging inputs? Can newly generated granule cells be excited coincident with active GABAergic conductances in contrast to mature neurons?

Forth, if there is GABAergic excitation and inhibition, what are the underlying mechanisms?

3 Methods

3.1 Slice preparation

Experiments were performed on heterozygous transgenic mice of both genders expressing the red fluorescent protein DsRed under the control of the doublecortin (DCX) promoter maintained in a C57Bl/6 background (Couillard-Despres et al. 2006). Coexpression of DsRed allows to visually identify adult-born premature granule cells in acute brain slices. In order to increase hippocampal neurogenesis, the mice were housed in groups of 4 to 10 animals at a 12:12 h light/ dark cycle in large cages (595x380x200 mm, Figure 3) with running wheels, tunnels and houses for at least 2 weeks prior to experiments, which were performed at the age of 5 to 11 weeks (mostly 8 to 10 weeks). The animals were anaesthetized with isoflurane (4% in O_2, Vapor, Draeger) and killed by decapitation in accordance with national and institutional guidelines. In order to increase cell viability, animals were exposed to oxygen-enriched atmosphere for 10 min prior to decapitation. The head was transferred into ice-cooled sucrose-based solution aerated with carbogen (gas mixture of 95% O_2 and 5% CO_2), fur and cranium were removed, olfactory bulb and cerebellum were cut off and the cerebrum was transferred into fresh ice-cooled solution. The two hemispheres were separated with a medial scalpel cut. On each hemisphere, a second cut removed a small dorsal part. The cut was optimized to guarantee healthy and intact dendrites of the granule cells. Subsequently, the two hemispheres were glued with the cut surface onto a small plate, transferred into a cutting chamber and immediately covered with ice-cooled cutting solution. Transverse 350-μm-thick hippocampal brain slices were cut with a velocity of 0.04 mm/s and a lateral vibrating amplitude of 1.8 mm using a VT1200 vibratome (Leica, Wetzlar, Germany; Geiger et al. 2002, Bischofberger et al. 2006). Slices were kept at 35°C for 30 min after slicing and subsequently stored at room temperature until experiments were performed.

Figure 3 **Environmentally enriched mouse cage with a mouse house, tunnels and a running wheel.**

3.2 Stereotaxic viral injections

In a second approach, dividing neuronal progenitor cells and their progenies were identified and stably labeled using a Moloney murine leukemia virus containing a green fluorescent protein (GFP) expression cassette under the control of the CAG promoter (Zhao et al. 2006). Viral injections were performed by Sébastien Sultan (University of Lausanne, group of Nicolas Toni) as previously described (Sultan et al. 2013). Mice were anesthetized with continuous isoflurane infusion using a calibrated anesthetic delivery machine. Mice were induced into anesthesia at a dose of 4% isoflurane, then maintained at a surgical plane by continuous inhalation of 2% isoflurane. Mice were then placed in a stereotaxic frame (Narishige Scientific Instruments, Tokyo, Japan). Final virus titers were 10^7-10^8 pfu/ml and 1.5 µl was injected into the dentate gyrus at the following coordinates from the Bregma: -2 mm antero-posterior, 1.75 mm lateral and -2.00 mm dorso-ventral, using a calibrated 5-µl Hamilton syringe fitted with a 33-gauge needle.

3.3 Identification of newborn granule cells

Electrophysiological experiments on acute brain slices were performed usually within 8 hours after slicing. Slices were placed into a transparent bath chamber and fixed with a nylon grid. The chamber was continuously superfused with artificial cerebrospinal fluid (ACSF, pH 7.4, equilibrated with 95% O_2/ 5% CO_2). The cells were visualized with

an infrared differential interference contrast (IR-DIC) microscope (Examiner.D1, Zeiss**,** Oberkochen, Germany) using a 40x objective (numerical aperture 0.8, Olympus, Tokyo, Japan). For video documentation, an IR camera (DAGE MTI VE-1000N, Chromaphor, Bottrop, Germany) and videocard (Hauppauge BT878, New York, USA) was used. Newly generated young granule cells were identified in the dentate gyrus by simultaneous detection of DsRed or GFP fluorescence using a cooled CCD camera system (SensiCam, TILL Photonics, now FEI Munich GmbH, Gräfelfing, Germany). The excitation light source (555 nm, Polychrome V, TILL Photonics) was coupled to the epifluorescent port of the microscope via a quartz light guide. The illumination intensity was reduced to about 10% by a neutral density filter to avoid bleaching and phototoxic damage of the cells. As DsRed fluorescence could outlast the DCX expression period, young granule cell were additionally identified by their small soma and the location at the inner border of the granule cell layer. Granule cells newly generated in the adult brain with input resistances (R_{in}) higher than 1.5 GΩ where shown to be immunopositive for PSA-NCAM (Schmidt-Hieber et al. 2004) which correlates in expression to DCX (Varea et al. 2011, Spampanato et al. 2012). Therefore, DCX^+ granule cells with a $R_{in} \geq 1.5$ GΩ were classified as young. Referring to previous publications, mature granule cells were restricted to a location on the outer border of the GCL and a $R_{in} \leq 400$ MΩ (Schmidt-Hieber et al. 2004).

3.4 Electrophysiology

Single cell recordings were performed on GCs of different developmental stages.

Mature granule cells were recorded with patch pipettes (3-6 MΩ) pulled from borosilicate glass tubings with 2.0 mm outer diameter and 0.5 mm wall thickness (Hilgenberg, Malsfeld, Germany; Flaming-Brown P-97 puller, Sutter Instruments, Novato, USA). The intracellular solution was based on $KMeSO_4$ with a Cl^--concentration of 6 mM resulting in an E_{GABA} of -69.8±1.3 mV (n=8) and a driving force from the holding potential (V_{hold} = -80 mV) of ~10 mV. These conditions were chosen to exclude falling below the physiological driving force (5.6 mV) from the resting potential (V_{rest}) of -83.0±0.4 mV (n=56) to the physiological E_{GABA} of –77.4±3.1 mV (n=6), as this would result in an underestimation of GABAergic depolarization in mature GCs.

Recordings of newborn young granule cells with high R_{in} have to be performed, especially in current-clamp configuration, with particular caution to be able to precisely measure both steady state potentials and fast voltage fluctuations. In contrast to the common procedures, pipettes (6-12 MΩ) were therefore pulled from thick-walled glass tubings with 2.0 mm outer diameter and 0.7 mm wall thickness. The relatively low capacitance (~5 pF) of these pipettes fastens the time course of the conducted current, which is essential for recordings of clearly overshooting APs in the very young cells. Furthermore, a tight connection (seal) of the glass pipette and the cell membrane is important to avoid current loss and shunting of the cell. A low seal resistance (R_{seal}) would depolarize V_{rest} and affect AP firing, as it can depolarize the AP threshold or even completely prohibit AP generation due to loss of inward currents mediated by voltage-gated Na^+-channels through the shunt. In order to obtain an R_{seal} of several GΩ, the pipettes were gently heat-polished on a micro-forge prior to use. The platinum wire of the micro-forge has to be covered with a small glass ball to avoid metal deposition on the pipette tip. For the polishing process it must be noted that polishing too weak is not sufficient to smoothen the tip surface. On the other hand, polishing too strong will make the glass border too round and result in an instable series resistance. For whole-cell recordings of young neurons in this study, the seal resistance was on average 32.4±1.2 GΩ corresponding to 8.2±0.6 times R_{in} (n=93). The AP threshold was determined from cells with R_{Seal} at least 5 times R_{in}. In all cells to which this criteria applied, V_{rest} was more negative than -60 mV (n=71). Therefore, cells with V_{rest} more depolarized than -60 mV were discarded. The holding potential (V_{hold}) was set to -80 mV close the average resting potential of the young and mature granule cells (-74.6±0.5 mV, n=132 and -83.0±0.4 mV, n=56, respectively). Recording pipettes were filled with a K-gluconate-based intracellular solution. The Cl^--concentration was set to 25 mM in order to obtain a GABA reversal potential comparable to perforated-patch measurements (whole-cell: -33.6±0.9 mV, n=12; perforated-patch: -36.7±1.9 mV, n=10; P=0.2341, Mann-Whitney U test).

Voltage signals and currents were measured with a Multiclamp 700B amplifier (Molecular Devices, Palo Alto, CA, USA), filtered at 1 and 10 kHz for current and voltage clamp, respectively, and digitized with 20 kHz using a CED Power 1401 interface (Cambridge Electronic Design, Cambridge, UK). Bridge balance was used to compensate the series resistance (R_S) in current clamp recordings ($R_S \approx$ 10-50 MΩ). In voltage clamp, series resistance was not compensated and experiments were

discarded if R_S changed by more than 20% during the recordings. All experiments were performed at 30-32 °C.

Data acquisition and analysis were achieved using a custom software (FPulse, U. Fröbe, Physiological Institute Freiburg) running under IGOR Pro 6.31 (WaveMetrics, Lake Oswego, Oregon) and the open source analysis software Stimfit (http://code.google.com/p/stimfit, C. Schmidt-Hieber, University College London).

3.5 Perforated-patch recordings of GABA reversal potentials

The non-invasive perforant-patch recording technique was used to determine GABA reversal potentials in hippocampal granule cells. Gramicidin within the pipette solution forms pores in the cell membrane patch under the pipette, which are permeable for small cations like Na^+ and K^+ but not for Cl^- (Akaike and Harata 1994, Ebihara et al. 1995). This allows the recording of GABAergic postsynaptic currents (GPSCs) without affecting the cellular Cl^- ion concentration (Figure 4).

For perforated-patch recordings, pipettes of 5-8 MΩ were pulled from borosilicate glass tubings. The pipette solution contained 40-100 µg/ml gramicidin, 0.2–0.4% dimethylsulfoxide (DMSO) and 50 µM Lucifer Yellow or Alexa 495 added to the intracellular K-gluconate-based solution used in whole-cell patch-clamp recordings. Every day, a new stock solution of gramicidin (mixture of gramicidins A, B, C and D) with 20-40 mg/ml dissolved in DMSO was prepared and sonicated for about 10 min. The intracellular solution was enriched with the fluorescent dye, filtered (0.2µm) and warmed up to ~35°C. After adding gramicidin, the solution was further sonicated for 5 min, filtered (0.45µm) and used for a maximum of 2 hours. The young cells have to be recorded with a high R_{seal} for which the use of thick-walled glass pipettes is essential. However, the small pipette volume reduces the diffusion of gramicidin inside the pipette tip. Therefore, the pipettes were tip-filled with standard internal solution and then back-filled with gramicidin-containing solution. The tip-fill was then blown out completely in the bath , far from slice surface. After rapid formation of a tight membrane seal, a 5-mV-voltage pulse was applied to monitor the decline of the access resistance. Resting membrane potential was monitored in the I=0 mode. Recordings were started after the establishment of an access resistance of 60-90 MΩ, usually about 10 min after seal formation. GABA-currents were evoked by extracellular stimulation in the granule cell layer (200 µs) in the presence of 10 µM NBQX, 25 µM AP5 and 2 µM

CGP54626. Stimulus-evoked GABAergic postsynaptic currents were recorded at different membrane potentials between -120 and -20 mV. For each cell, GPSC-amplitudes were measured from averages of 5-10 traces and plotted against holding potential. The reversal potential of GABA receptor-mediated currents (E_{GABA}) was determined by an exponential fit intersecting the x-axis.

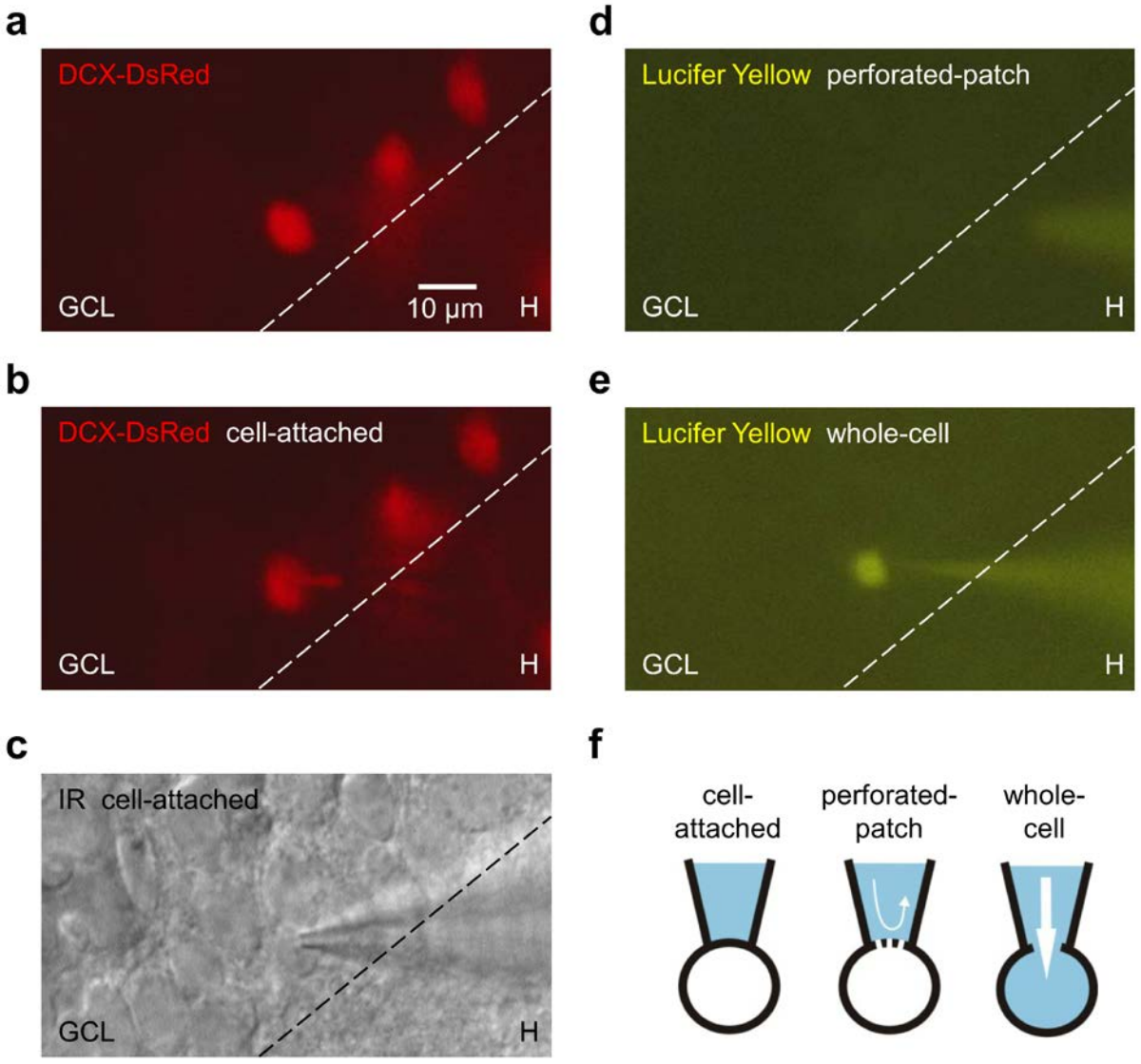

Figure 4 **Gramicidin perforated-patch recordings in DCX-DsRed⁺ young hippocampal granule cells of the adult mouse brain. a-e,** Gramicidin perforated-patch recordings of the GABA reversal potential in a young GC. DsRed-fluorescence of a DCX-DsRed⁺ cell before patching (**a**) and in cell-attached mode (**b**). IR-DIC image of the recorded cell (**c**). Lucifer Yellow is restricted to the pipette during perforated-patch configuration (**d**), but clearly visible in the soma in whole-cell mode (**e**). GCL, granule cell layer. H, hilus. **f,** Scheme of different recording modes showing the separation of pipette and intracellular solutions in the perforated-patch configuration.

3.6 Extracellular synaptic stimulation

For stimulation of synaptic inputs, 2-5 MΩ pipettes filled with HEPES-buffered Na^{2+}-rich solution were used to apply brief negative current pulses (5-100 µA, 200 µs). In order to stimulate GABAergic interneurons, the pipettes were placed in the outer third of the granule cell layer (GCL), approximately 100 µm laterally to the recorded cell. For stimulation of axonal fibers in the molecular layer (ML), the pipettes were placed approximately in the middle third of the ML radial to the recorded cell at a distance of ~100 µm.

For recordings of GABAergic synaptic inputs, $GABA_A$-receptor-mediated synaptic transmission was isolated by application of 10 µM NBQX (2,3-dioxo-6-nitro-1,2,3,4-tetrahydrobenzo[*f*]quinoxaline-7-sulfonamide), 25 µM AP5 (D-(-)-2-amino-5-phosphonopentanoic acid), and 2 µM CGP54626. Gabazine (SR95531) was used at concentrations of 0.2 and 10 µM for a half-maximal and complete block of $GABA_A$-mediated currents, respectively.

The impact of GABAergic synaptic transmission on cell excitability of newborn young GCs was examined using three different stimulation paradigms.

GABA-induced spiking

The modulation of ML-input by local interneurons was investigated using a combination of GCL- and ML-stimulation with either a burst of 8 stimuli at 50 Hz (GCL, 4-10 µA, 200 µs) or 2 pulses separated by 10 ms (ML, 10-100 µA, 200 µs). The stimulations were applied either individually or paired with 30 ms delay between GCL- and ML-stimulation. “ML-GCL-pairing high” was performed with a 3-times stronger GCL-stimulation intensity whereas ML-stimulation-strength remained unchanged. Each stimulation intensity was applied 10 times to calculate AP firing probability.

Timing-dependent spiking

To evaluate the effect of the precise timing of GABAergic postsynaptic potentials (GPSPs) and additional excitatory PSPs (EPSPs), GABAergic synaptic inputs were isolated using NBQX, AP5 and CGP. Glutamatergic inputs were mimicked using a ~20 mV mock EPSP induced by a current injection of 30-80 pA for 10 ms. The mock EPSP was applied in combination with a stimulation in the GCL (2 or 8 stimuli at 50 Hz, 10 or 50 µA, 200 µs). The relative timing of mock EPSP and stimulation was shifted in each trial and ranged from 1 s before stimulation to 1.5 s after stimulation start.

GABA-dependent excitation and shunting inhibition

In order to investigate the mechanism underlying GABA-dependent firing and AP-block, GCL-burst-stimulation was applied with subsequent mock EPSP induction. For each newborn GC the minimum stimulus intensity to induce a GPSP was determined (4-10 µA). The GCL-stimulation intensity was then increased by this threshold over 10 following stimulations. The applied intensity range covered the full spectrum of GABAergic conductances. Each stimulation intensity was applied 5 times and AP firing probability was calculated. The same stimulation intensities were used in voltage-clamp mode in the same cells and GPSC amplitudes were measured from averages of 5-10 traces.

Stimulation protocols were repeated at a frequency of 0.04 Hz.

3.7 Data analysis

Intrinsic cell properties

Intrinsic properties were determined within the first minutes in whole-cell configuration. Membrane potentials were measured without correction for liquid junction potentials. Resting membrane potentials were measured in the I=0 mode. The input resistance and the membrane capacitance were determined in voltage clamp from the current response to a negative voltage pulse (-5 mV, 500 ms) from a holding potential of -80 mV. The capacitive current transients from mature granule cells showed a biexponential decay time course probably corresponding to a somatic and a dendritic compartment. Measurement of the amplitude-weighted decay time constant (τ_w = 1.18±0.06 ms) and the series resistance (R_S = 17.4±0.8 MΩ) revealed a membrane capacitance of 69±5 pF (n=10). By contrast, data from young neurons could be well fitted with a fast monoexponential function with τ = 831±94 µs. Measurement of the R_S = 42.4±2.7 MΩ revealed a relatively small average capacitance of 19.2±1.5 pF (n=23). The membrane time constant (τ_m) was estimated in current-clamp mode by fitting a monoexponential function to the voltage decay after a small 1-s-current-pulse leading to approximately 5 mV hyperpolarization. Action potential properties were determined from the first spike elicited by a 500-ms-step protocol with 1 and 10 or 50 pA steps for young DCX^+ neurons and mature granule cells, respectively. Action potential threshold was estimated from cells of 1.5 to 10 GΩ, covering the full R_{in} range used for E_{GABA} measurements. The APs were filtered using a 2nd order Savitzky-Golay-

filter at 1 kHz and threshold was determined as the first minimum in the slope within 2 ms before a slope of 10 V/s was reached. On average, the slope minimum of the AP threshold was 1.5±0.3 V/s (n=13). Stimulation artifacts were blanked in all voltage clamp figures.

Synaptic conductance

To estimate the GABA-mediated synaptic conductances (g_{syn}) the voltage drop ($\Delta V_{Rs} = R_S \cdot \Delta I$) due to series resistance was considered. Therefore, the conductance of synaptic currents was calculated using the following equation:

$$g_{syn} = \frac{\Delta I}{(V_{hold} - \Delta V_{Rs}) - E_{GABA}} \quad (1)$$

with V_{hold} = -80 mV and E_{GABA} = -35 mV and -75 mV for young and mature granule cells, respectively. Stimulation-induced synaptic conductances were calculated at the time of mock EPSP current injection (30-40 ms after burst).

AP probability

AP probabilities were averaged in bins of 1 nS and the dependence on the synaptic conductance (g) was fitted with the product of a sigmoidal rise and decay:

$$f(g) = A_{max} \cdot \frac{1}{\left(1+e^{(g1-g)/slope1}\right)} \cdot \frac{1}{\left(1+e^{(g-g2)/slope2}\right)} \quad (2)$$

The effect of shunting inhibition onto subthreshold responses evoked by mock EPSPs was analyzed by fitting the measured data with equations developed within the framework of an electrical single compartment model.

Single compartment model

According to the data, newly generated DCX-positive granule cells show a small capacitance and a remarkably high electrical input resistance. Furthermore, fitting the decay of the membrane potential after the mock EPSP with a monoexponential function (τ_0 = 95.8±17.9, n=10) revealed values similar to the membrane time constant measured after 1-s-pulses (τ_m = 101.5±12.9 ms, n=10, P=0.4316, Wilcoxon signed rank test). The absence of a rapid transient component after the short current pulse indicates that the young cells lack pronounced charge redistribution and are electronically compact (Schmidt-Hieber et al. 2007). Therefore, a single-compartment model corresponding to a simple leaky integrator neuron was used to computationally model newly generated young granule cells.

An analytical solution of the single compartment model was derived to fit the decay time constant, peak amplitude, and half duration of mock EPSPs. The time constant of a charging leaky capacitance is well known as $\tau_0 = R \bullet C = C/G$. As the resting membrane conductance $G_{in} = 1/R_{in}$ is increased during a constant steady state GABAergic synaptic conductance to $G_{in}^s = 1/R_{in} + g$, the membrane time constant during shunt (τ_s) reduces as a function of the synaptic conductance g according to:

$$\tau_s = \tau_0 \cdot \frac{G_{in}}{G_{in} + x \cdot g} \quad (3)$$

with G_{in} (0.26 nS, n=10) calculated from the experimentally determined average input resistance. This analytical function was used to fit the measured τ_s with x as the only free parameter. Alternatively, for theoretical predictions, the scaling factor x was fixed to $x = 1$.

For analysis of the mock EPSP amplitude on top of the GPSP, data above 1 nS were corrected considering additional voltage-dependent conductances activated at -40 mV which reduce the mock EPSP amplitude to 84% relative to mock EPSPs evoked at -80 mV (n=6). The peak voltage amplitude at Δt = 10 ms was assumed as:

$$V(\Delta t) = V_0(1 - e^{-\Delta t/\tau_0}) \quad (4)$$

with the steady state voltage amplitude calculated from $V_0 = R_{in} \bullet \Delta I$. Thus, the relative reduction of the shunted peak amplitude $V^s(\Delta t)$ can be calculated as:

$$\frac{V^s(\Delta t)}{V(\Delta t)} = \frac{V_0^s\,(1 - e^{-\Delta t/\tau_s})}{V_0\,(1 - e^{-\Delta t/\tau_0})} \quad (5)$$

The ratio of V_0^s divided by V_0 can be directly replaced by the ratio of input conductances. Furthermore, using the scaling factor x for the shunting conductance and the shunted decay time constant τ_s as defined by equation (3), the following function was derived to fit the relative reduction of the shunted EPSP amplitude with x as the only free parameter:

$$\frac{V^s(\Delta t,g)}{V(\Delta t)} = \frac{G_{in}\,(1 - e^{-\Delta t/\tau_s})}{(G_{in} + x \cdot g)\,(1 - e^{-\Delta t/\tau_0})} \quad (6)$$

Finally, the half duration (t_{50}) of the mock EPSP was analyzed and compared to the theoretical prediction, which was calculated as the interval between time t_1 when the

voltage reached 50% of its maximum during rising phase and the time t_2 when it decayed back to 50% of its peak amplitude:

$$t_{50} = t_2 + (\Delta t - t_1) \quad (7)$$

The time point t_1 was derived according to equation (4) as

$$V^s(t_1) \triangleq \frac{1}{2} V_s(\Delta t) \quad \Rightarrow \quad (1 - e^{-\frac{t_1}{\tau_s}}) = \frac{1}{2}(1 - e^{-\frac{\Delta t}{\tau_s}}) \quad (8)$$

$$\Rightarrow \quad t_1 = -\tau_s ln \frac{1}{2}(1 + e^{-\frac{\Delta t}{\tau_s}}) \quad (9)$$

The time point t_2 was calculated from the exponential decay after the peak $V^s(\Delta t)$ as:

$$V^s(\Delta t) e^{-t_2/\tau_s} \triangleq \frac{1}{2} V^s(\Delta t) \quad \Rightarrow e^{-t_2/\tau_s} = \frac{1}{2} \quad (10)$$

$$\Rightarrow \quad t_2 = -\tau_s \, ln \frac{1}{2} \quad (11)$$

Thus, according to equation (7), (9) and (11) the half duration was derived as:

$$t_{50} = \Delta t + \tau_s \cdot \ln(1 + e^{-\Delta t/\tau_s}) \quad (12)$$

using the shunted decay time constant τ_s which is dependent on *g* and the scaling factor x as calculated by equation (3).

The scaling factors of the three fitted parameters were finally averaged. As all three parameters were determined from the same sample size, the means were averaged to obtain a grand mean. The standard deviations were averaged by the mean of the single variances according to the following equation:

$$\sigma_{total} = \sqrt{\frac{{\sigma_1}^2 + {\sigma_2}^2 + {\sigma_3}^2}{3}} \quad (13)$$

with σ_1, σ_2, and σ_3 obtained from the scaling factors for the relative decay τ, amplitude and the half duration, respectively.

Statistical analysis

Statistical analysis was performed with GraphPad Prism 6 using a two-sided Mann-Whitney or a Wilcoxon matched-pairs signed rank test for unpaired and paired data, respectively. The Kruskal-Wallis test was used to compare more than two samples.

The significance level was set to $P < 0.05$. Average data were given as mean±SEM if not stated otherwise and fitted parameter values as mean±SD.

3.8 Immunohistochemistry

Immunohistochemical analysis of GCs was performed as described previously (Schmidt-Hieber et al. 2004, Couillard-Despres et al. 2006). Cells were filled with biocytin (2 mg/ml) during whole-cell recording and, after closure of the membrane by formation of an outside-out patch, stored at room temperature for at least one hour. Acute brain slices were subsequently fixed overnight in 4% paraformaldehyde, washed and then incubated overnight with 5% normal donkey serum, 0.3% Triton X-100 (Sigma-Aldrich) and the primary antibody goat anti-Doublecortin 1:500 (DCX C-18, sc-8066, Santa Cruz Biotechnology, Inc.). Afterwards, the secondary antibody (Alexa Fluor 488 donkey anti-goat, 1:500, A11055, Molecular Probes) was applied together with fluorescein isothiocyanate-conjugated avidin-D (2 µl/ml, Vector) and 0.3% Triton X-100 for 24 h at 4 °C. After washing, the slices were embedded in Prolong Gold (Molecular Probes). Fluorescence labeling was analyzed with a confocal laser scanning microscope (LSM 700, Zeiss).

3.9 Solutions

ACSF

For electrophysiological recordings, slices were continuously superfused with artificial cerebrospinal fluid (ACSF) containing (in mM): 125 NaCl, 25 $NaHCO_3$, 25 glucose, 3 KCl, 1 NaH_2PO_4, 2 $CaCl_2$, 1 $MgCl_2$ (pH 7.4, equilibrated with 95% O_2/ 5% CO_2, Osmolarity 314-325 mOsm).

Sucrose

For cutting and storage, a sucrose-based solution was used, containing (in mM): 87 NaCl, 25 $NaHCO_3$, 2.5 KCl, 1.25 NaH_2PO_4, 75 sucrose, 0.5 $CaCl_2$, 7 $MgCl_2$ and 10 glucose (equilibrated with 95% O_2/ 5% CO_2, Osmolarity 325-328 mOsm).

Pipette Solutions

Newborn young granule cells were recorded with patch pipettes filled with an intracellular solution containing (in mM): 120 K-gluconate, 21 KCl, 2 $MgCl_2$, 2 Na_2ATP,

0.3 NaGTP, 10 HEPES, 10 EGTA, 0-1 Na_2-phosphocreatine, 0-0.01 Spermine, 0-5 mg/ml Biocytin (adjusted to pH 7.3 with KOH, Osmolarity 305-310 mOsm).

Mature granule cells were recorded with pipettes filled with a solution containing (in mM): 140 $KMeSO_4$, 2 KCl, 2 $MgCl_2$, 2 Na_2ATP, 0.3 NaGTP, 10 HEPES, 10 EGTA, 1 Na_2-phosphocreatine, 2 mg/ml Biocytin (adjusted to pH 7.3 with KOH, Osmolarity 305-310 mOsm).

Extracellular stimulation pipettes were filled a solution containing (in mM): 155 NaCl, 2,5 KCl, 2 $CaCl_2$, 1 $MgCl_2$, 5 HEPES (adjusted to pH 7.3 with NaOH, Osmolarity 320 mOsm).

Drugs

For all drugs a stock solution was prepared and stored at -20°C (). Each day the drugs were dissolved in ACSF before use. All chemicals were obtained from Tocris (Essex, England), Sigma-Aldrich (Steinheim, Germany), Merck (Darmstadt, Germany), Molecular Probes (Göttingen, Germany) or Vector (Burlingame, USA).

Drug	Dissolved in	Stock concentration (mM)	Final concentration (µM)
SR95531	water	10	10
NBQX	water	20	10
AP5	DMSO	50	25
CGP54626	DMSO	10	1

Table 1 **Stock and final concentrations of drugs used in electrophysiological experiments.**

4 Results

4.1 Input resistance serves as an indicator of the maturational state

GABAergic synaptic signaling in newly generated young granule cells was studied in adult mice using two technical approaches in order to identify newborn neurons in acute brain slices.

First, transgenic mice were used which express the red fluorescent protein DsRed under the control of the doublecortin (DCX) promoter, labeling young granule cells within 3 weeks post-mitosis (Couillard-Despres et al. 2006). The DCX^+ young neurons showed an immature morphology with basal dendrites and a small apical dendritic tree, but had already long axons into the CA3 area (Figure 5a, d). In all cells, somatic current injections elicited a typical firing pattern with a low-threshold single action potential with a rheobase of 7.1±0.5 pA (n=93; Figure 5b, e). Small hyperpolarizing current steps revealed a slow membrane time constant known for newly generated neurons (τ_m = 117.1±4.7 ms, n=93; Figure 5c, f; Schmidt-Hieber et al. 2004, Couillard-Despres et al. 2006). Basic electrophysiological properties and electrical input resistance (R_{in} = 4.75±0.26 GΩ, range ~1.5-18 GΩ, n=132) were similar to what was reported previously for DCX^+ and PSA-$NCAM^+$ newly generated granule cells in the adult hippocampus (Overstreet et al. 2004, Schmidt-Hieber et al. 2004, Couillard-Despres et al. 2006). Mature GCs with input resistances of 201.6±12.1 MΩ (n=56) show in contrast a fully developed dendritic tree, repetitive firing and a fast membrane time constant (rheobase = 126.8±7.8 pA, τ_m = 24.8±1.3 ms, n=50, Figure 5g-i).

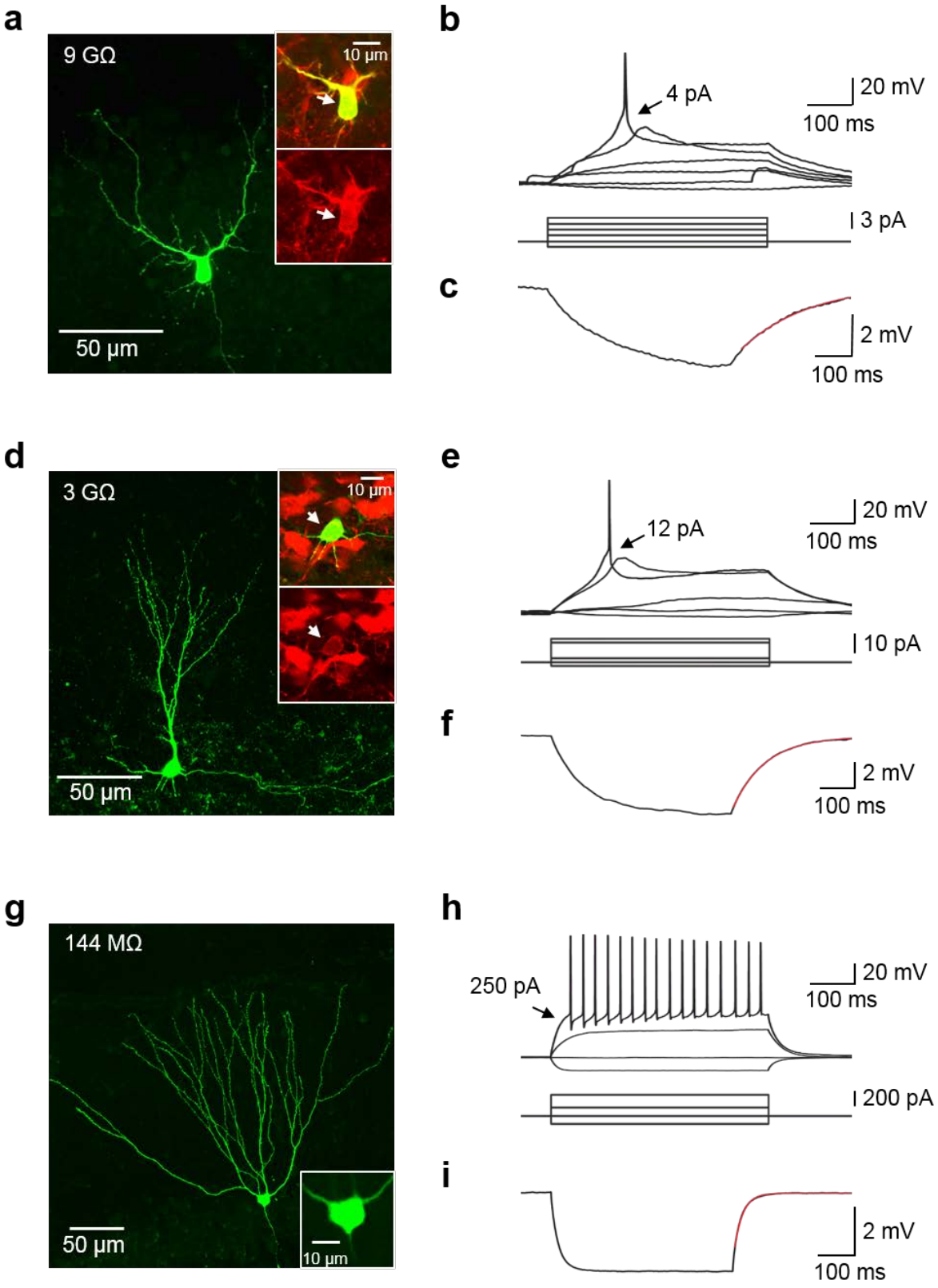

Figure 5 **Morphology and firing pattern of young and mature granule cells in the adult hippocampus.**

The R_{in} mainly depends on the specific membrane conductance as well as total membrane area. Therefore, it may serve as an indicator of the maturational stage of the recorded cell. Figure 6 shows the strong correlation of the input resistance with several active and passive properties of immature $DsRed^{+}$ (red) and mature $DsRed^{-}$ (black) GCs. The resting membrane potential was remarkably similar between young and mature GCs (Figure 6a, -74.6±0.5 mV, n=132 vs. -83.0±0.4 mV, n=56). In contrast, substantial maturational changes were observed for the membrane time constant and the rheobase as already indicated above (Figure 6b and c). Furthermore, the rising slope of the APs, which strongly depends on the density of voltage-activated Na^{+}-channels, severely increases with the maturation of the GCs (Figure 6d, 80.9±4.6 V/s, n=93 and 235.2±4.4 V/s, n=50 for young and mature GCs, respectively). These results indicate that the input resistance can serve as a good reference of the maturational state of an adult-born granule cell.

Figure 5 **a,** Confocal z-projection of a biocytin-filled (green) newborn granule cell with an input resistance of 9 GΩ. Small images of immunohistochemical stainings show double-labeling with strong DCX expression (red). **b,** Isolated Ca^{2+}-spike and AP induced by somatic current injection of a 9 GΩ granule cell. Lowest current necessary for AP generation is indicated. **c,** Decay after a small hyperpolarization revealed slow membrane time constant (τ = 186 ms, monoexponential fit in red). **d,** Same as **a** for a 3 GΩ granule cell showing slightly advanced dendritic maturation and weaker DCX expression. **e,** Firing pattern of the cell in **d**. **f,** Same as **c** for the cell in **d** showing faster decay time constant (τ = 94 ms). **g,** Morphology of a mature DsRed-DCX^{-} granule cell. **h,** Mature firing pattern for the cell in **g** requires high current injection. **i,** Decay revealed a fast τ of 23 ms.

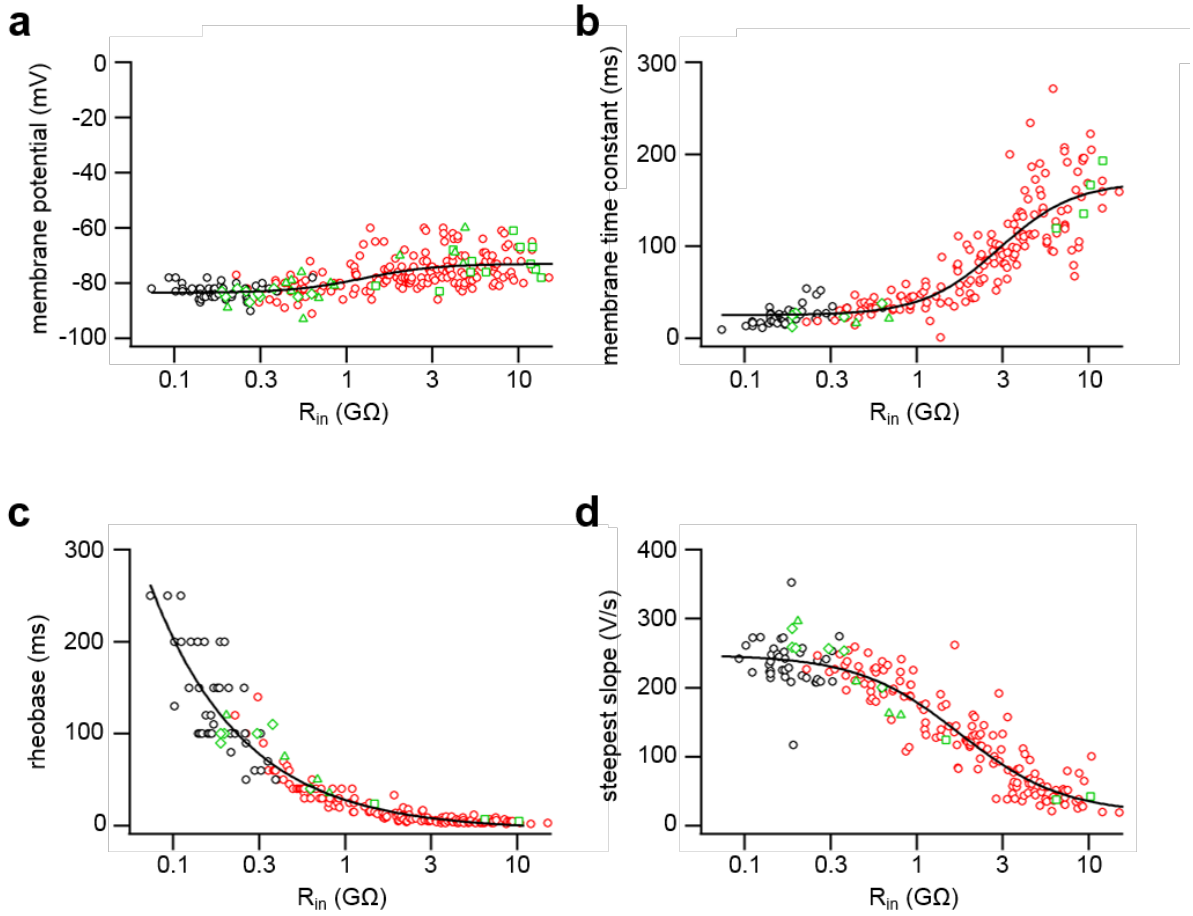

Figure 6 **Passive and active properties of developing granule cells change with maturation. a-d,** Semi-logarithmic plots of resting membrane potential (**a**), membrane time constant (**b**), rheobase (**c**) and steepest slope (**d**) of DsRed^{+} young (red), DsRed^{-} mature (black) granule cells and GFP^{+} birth-dated cells (green, Square, 2 weeks post injection (wpi). Triangle, 3 wpi. Diamond, 4 wpi). Lines represent sigmoidal (**a, b, d**) or double exponential (**c**) fits.

As a second approach, birth-dating of newborn neurons in the adult brain was achieved using a retroviral approach in order to label dividing cells during mitosis by the sustained expression of GFP. Electrophysiological recordings were performed on GFP^+ cells at 2, 3 and 4 weeks post injection (wpi, Figure 7, Table 2). Membrane potential, membrane time constant, steepest slope of action potentials and rheobase correlate to R_{in} comparable to DCX-$DsRed^+$ cells (Figure 6, green data points). Two week-old GFP-labeled neurons were similar to DCX-$DsRed^+$ cells in their active and passive properties, consistent with a stable DCX expression in all immunohistochemically analyzed cells 2 wpi (Figure 7a, Table 2, n=9). At 3 wpi, the granule cells were diverse in terms of cellular properties as well as DCX expression, indicating a nonuniform and cell specific tempo of maturation (Figure 7b, Table 2). At 4 wpi, both matured electrophysiological properties and missing DCX expression make them comparable to mature granule cells, consistent with previous publications (Figure 7c, Table 2, Brown et al. 2003, Overstreet-Wadiche and Westbrook 2006).

Wpi	V_m (mV)	R_{in} (GΩ or MΩ)	τ_m (ms)	Steepest slope (V/s)	DCX^+ cells	E_{GABA} (mV)
2	-73.1±1.9 (-61, -83) [12]	7.9±1.1 GΩ (1.5, 12.4) [13]	153.6±16.4 (119, 193) [4]	68.1±28.0 (38.0, 124) [3]	100% [9]	-34.9±1.7 (-31.4, -37.0) [3]
3	-78.1±2.1 (-60, -93) [15]	1.6±0.5 GΩ (0.206, 4.9) [14]	25.8±7.0 (16.3, 39.6) [3]	180.1±36.5 (72.4, 296) [5]	0.43% [7]	-59.2±11.0 (-38.0, -75.0) [3]
4	-83.9±0.5 (-82, -87) [11]	318.1±39.0 MΩ (189, 624) [12]	25.1±4.1 (12.5, 37.9) [5]	251.9±11.5 (200, 285) [6]	0% [4]	-59.6 [1]

Table 2 **Intrinsic properties of adult-born GFP^+ cells from 2 to 4 wpi.** Given are mean±SEM, the range as the lowest and highest value in parenthesis and the n in square brackets.

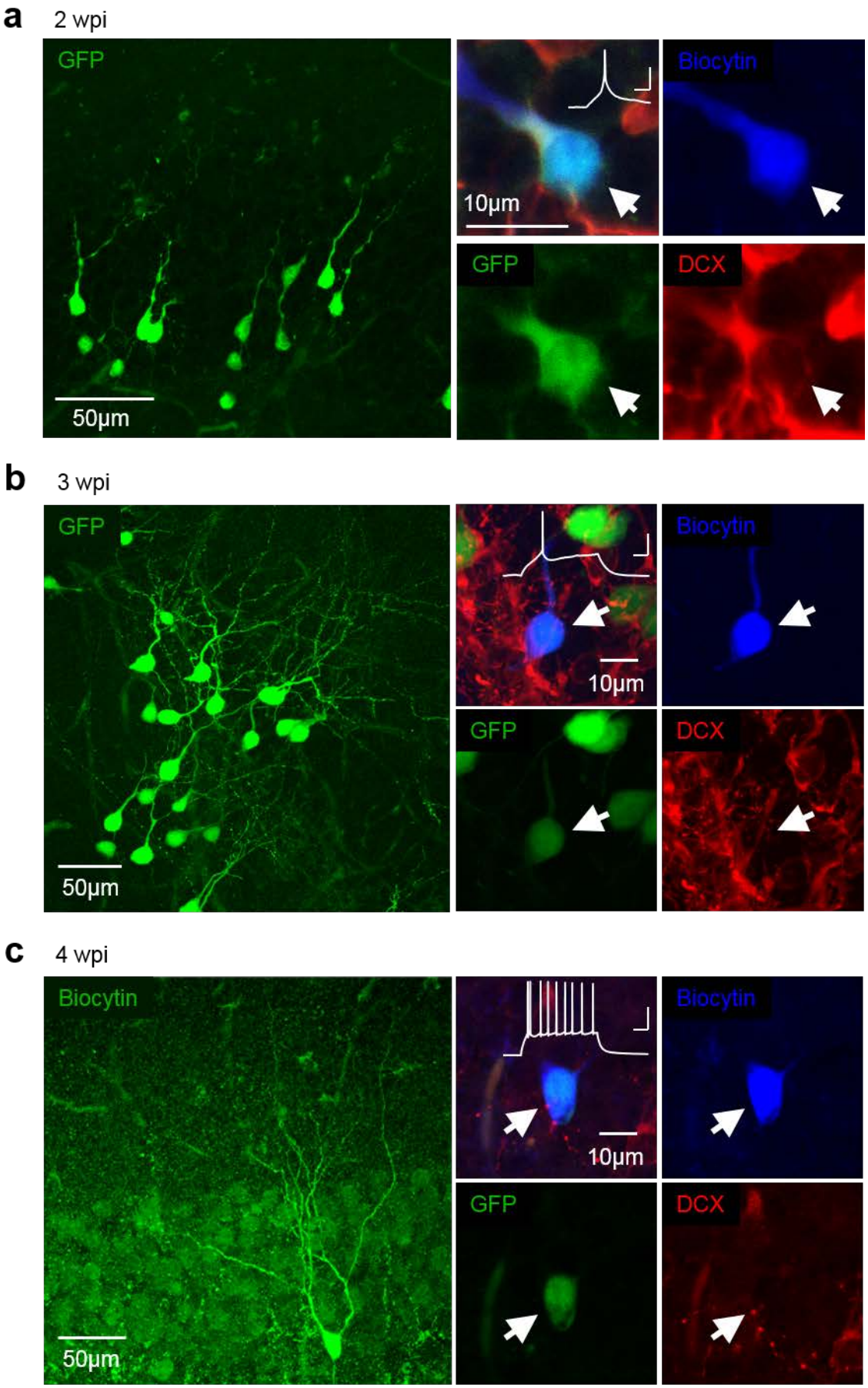

Figure 7 **Newborn hippocampal granule cells loose DCX expression at 3 weeks of age.**

4.2 Depolarizing E_{GABA} correlates with DCX expression in young GCs

Newly generated dentate gyrus GCs were reported to show a depolarized $GABA_A$-reversal potential (E_{GABA}) due to an enhanced expression of the chloride inward transporter NKCC1 and the lack of KCC2-dependent chloride ion extrusion (Ge et al. 2006). In order to measure the reversal potential of GABAergic synaptic inputs in young and mature granule cells, extracellular stimulations were applied in the GCL in the presence of pharmacological blockers for glutamatergic synaptic transmission (Figure 8). Gramicidin perforated-patch recordings were performed on GFP^+ cells at 2, 3 and 4 wpi and compared to unlabeled mature cells located at the outer border of the granule cell layer (GCL). The data show that E_{GABA} is depolarizing at 2 wpi (-34.9±1.7 mV, n=3, Figure 8a-c) and hyperpolarizes with maturation to -77.4±3.1 mV (n=6, Figure 8c), consistent with previous publications (Ge et al. 2006). The intermediate cells of 3 to 4 weeks, however, did not form a homogeneous population but covered a broad spectrum for E_{GABA}, comparable to the broad range of input resistances (Figure 8c, Table 2). Notably, the reevaluation on a single cell level revealed that depolarizing E_{GABA} was restricted to DCX-positive young granule cells (Figure 8c, orange data points).

In order to explore this hypothesis in more detail, an extensive analysis of E_{GABA} was performed using DCX-$DsRed^+$ transgenic mice (Figure 8d-h). As shown in Figure 8h, E_{GABA} correlates with R_{in} and can be fitted with a sigmoidal function ($R^2 = 0.8857$). The top plateau formed by neurons with high R_{in} revealed an E_{GABA} with mean±SD of -34.6±4.2mV in young DCX^+ GCs (n=10), similar to what was reported for $POMC^+$ and PSA-$NCAM^+$ cells in adult mice (Tozuka et al. 2005, Karten et al. 2006, Chancey et al. 2013). This is substantially more depolarized than the resting potential (V_{rest} = -74.6±0.5 mV, n=132). In contrast, DCX^- mature cells show an E_{GABA} close to resting potential (E_{GABA} = -76.1±2.8 mV (mean±SD), V_{rest} = -83.0±0.4 mV, n=56, Figure 8f, g). Together, these results show that the E_{GABA} of newly generated young granule cells is depolarized to about -35 mV. With proceeding synaptic and dendritic maturation and concomitant loss of DCX expression, E_{GABA} rapidly drops to mature values close to resting potential.

Figure 7 **a-c,** Confocal z-projection of GFP^+ neurons (left), biocytin filled somata with GFP and DCX expression (right) as well as corresponding firing pattern induced by current injection of newly generated granule cells at 2 (**a**), 3 (**b**), and 4 (**c**) weeks post injection.

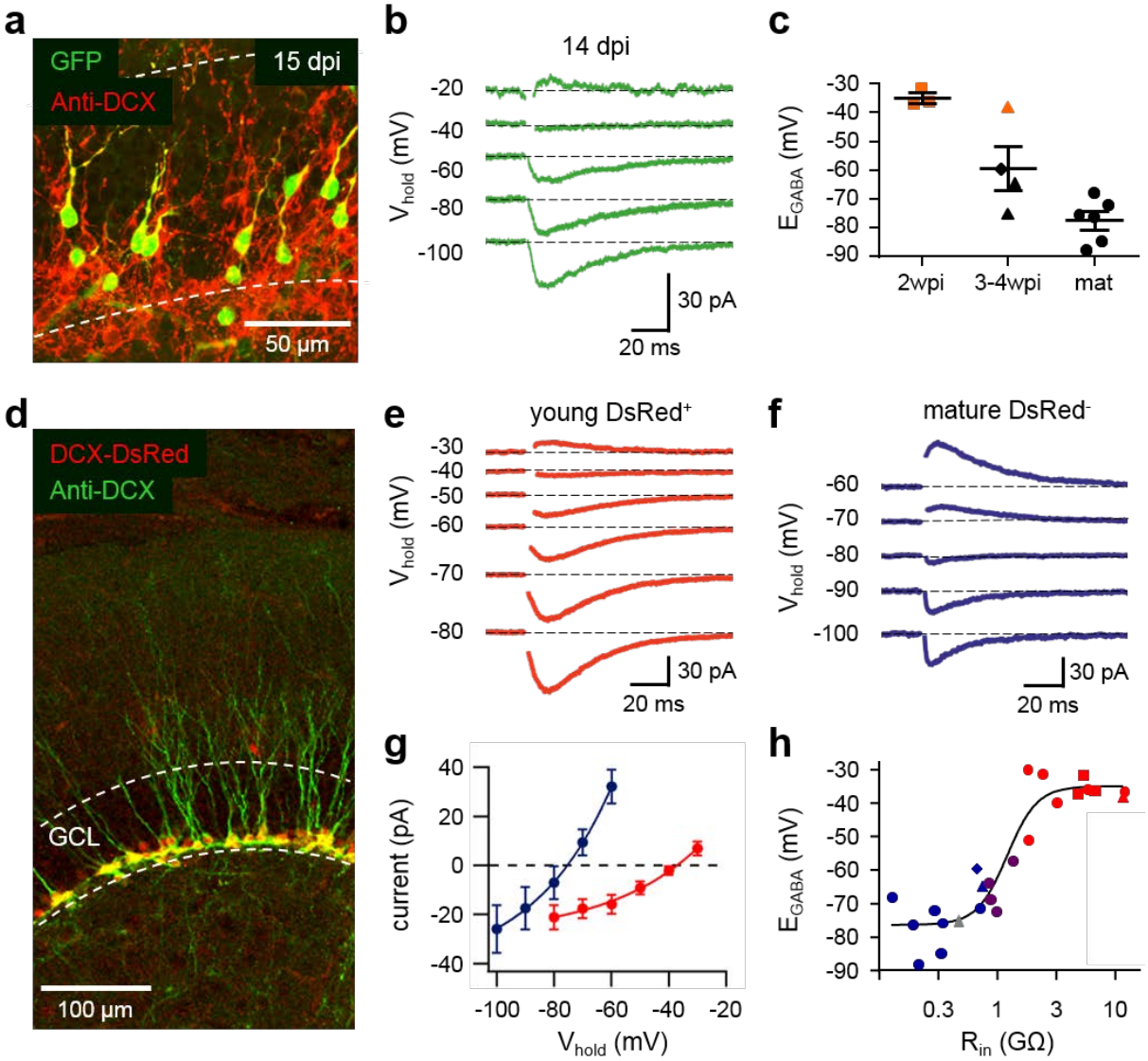

Figure 8 **Depolarizing GABA correlates with DCX-expression in hippocampal granule cells. a,** Newborn granule cells express DCX 15 days after virus injection. **b,** Gramicidin-perforated-patch recordings of GPSCs in a granule cell at 14 days post injection (dpi). GPSCs were evoked by extracellular stimulation of GABAergic fibers in the granule cells layer in the presence of NBQX and AP5 at holding potentials indicated on the left. **c,** E_{GABA} hyperpolarizes with maturation, but is most depolarized (~-35 mV) as long as doublecortin (DCX) is expressed (orange) independent of cell age. Wpi, weeks post injection. Square, 2 wpi. Triangle, 3 wpi. Diamond, 4 wpi. Circle, mature. **d,** DCX-DsRed$^+$ granule cells (red) express DCX protein (green), consistent with a young developmental stage of less than 3 weeks post-mitosis. GCL, granule cell layer. **e, f,** Gramicidin-perforated-patch recordings of GABAergic postsynaptic currents (GPSCs) in a young (**e**) and mature (**f**) granule cell. **g,** The average amplitudes of GPSCs from young (red) and mature (blue) granule cells were plotted against holding potential and fitted with an exponential function. **h,** The reversal potential of GPSCs (E_{GABA}) in granule cells is plotted against input resistance (R_{in}) indicating that DCX$^+$ young granule cells (red) show a more depolarized reversal potential than DCX$^-$ granule cells (blue). After loss of DCX expression, E_{GABA} rapidly approaches mature levels. Purple, intermediate DsRed$^+$ cells with R_{in} < 1.5GΩ. Gray, DCX expression not identified.

4.3 GABAergic control of action potential firing

Can depolarizing GABA induce action potential firing in newly generated young granule cells of the adult brain? To address this question, gramicidin perforated-patch recordings of AP firing were obtained from young DCX-DsRed$^+$ granule cells, which were known to show mainly GABAergic PSCs (Esposito et al. 2005, Ge et al. 2006). Synaptic inputs were evoked by stimulation of molecular layer (ML) fibers and synaptic inputs in the granule cell layer (GCL, Figure 9a). Using a short double pulse in the ML, APs were generated with a very low firing probability of 5.0±4.5% (n=5, Figure 9b, c). Similarly, low burst stimulation of the GCL with 8 pulses at 50 Hz induced an apparent depolarization but failed to generate action potentials in the young cells (Figure 9b, d). However, paired application of GCL with subsequent ML stimulation very efficiently evoked action potentials with a firing probability of 84.0±7.5% (n=5, Figure 9b, e). Remarkably, a three-fold increase in GCL stimulation strength (ML-GCL pairing high) evoked more rapid depolarization, but inhibited AP firing (Figure 9b, f).

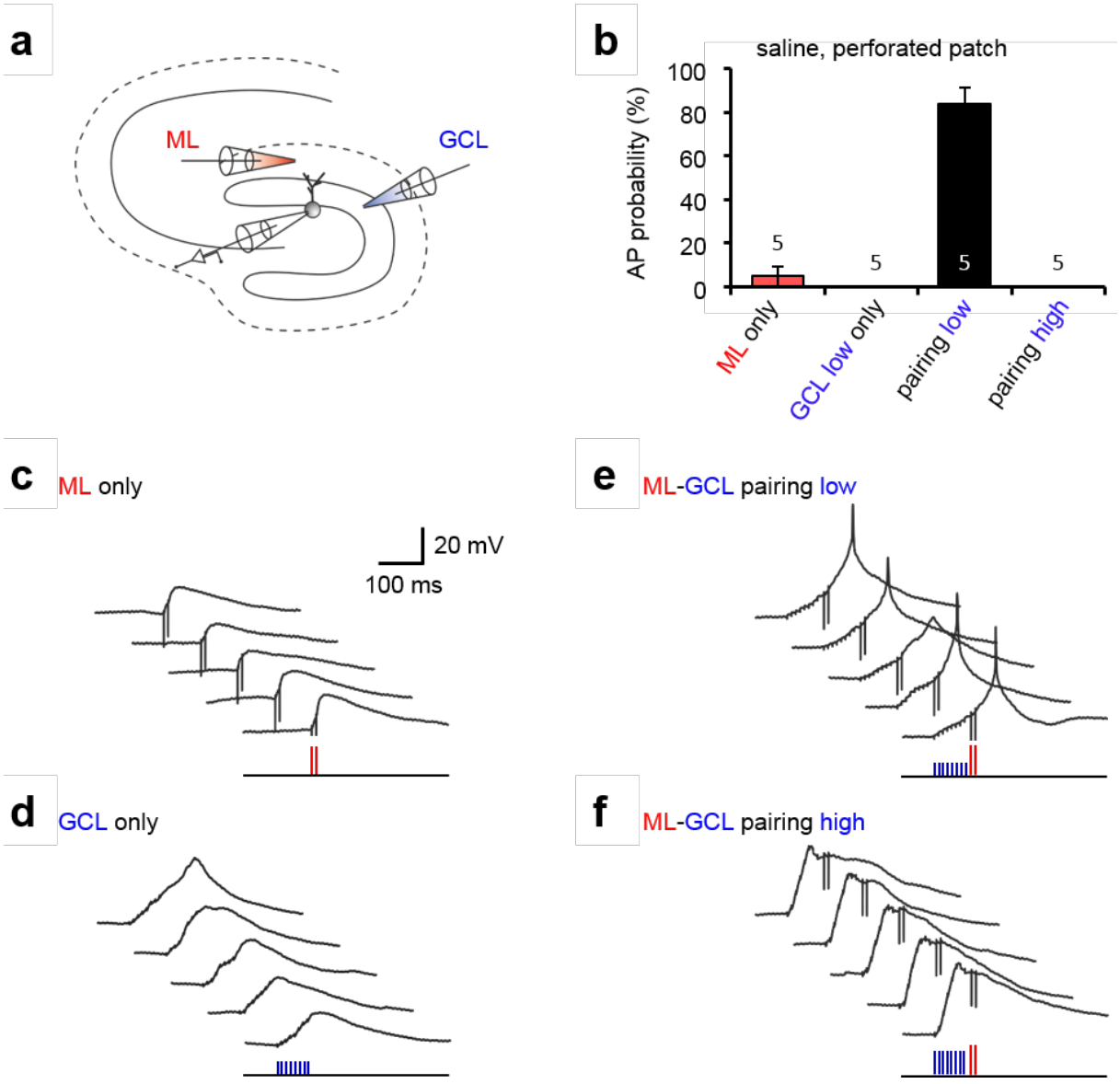

Figure 9 **Gramicidin perforated-patch recordings of AP firing in newborn young granule cells. a,** Scheme depicting the position of the recording electrode and the stimulation electrodes in the molecular layer (ML, red) and granule cells layer (GCL, blue). **b,** Firing probability in different conditions, showing that pairing of ML and low GCL stimulation drove more effectively AP generation in young granule cells than either stimulation alone. High GCL stimulation effectively inhibited subsequent AP firing. **c-f,** Five consecutive postsynaptic responses of a young GC to electrical stimulation of ML and GCL synaptic inputs (n=5). **c,** Subthreshold PSPs induced by a double pulse in the ML (100 Hz, 200 µs, red). **d,** Subthreshold PSPs induced by a burst stimulation in the GCL (8 times at 50Hz, 200 µs, blue). **e,** Pairing of ML and GCL stimulation effectively boosted AP firing. **f,** A 3-fold increase in GCL stimulation intensity inhibits AP generation.

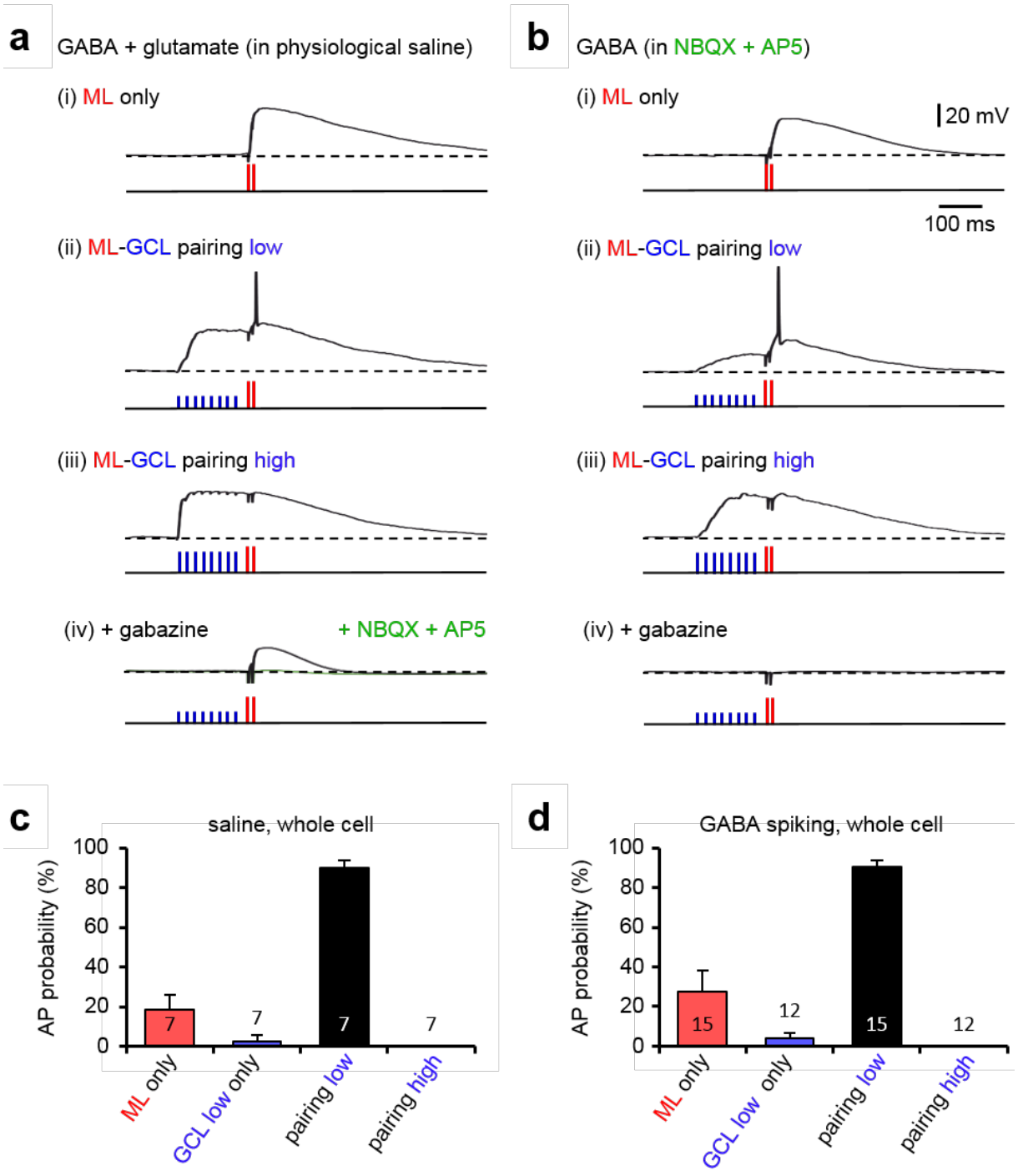

Figure 10 **Bidirectional GABAergic control of action potential firing in immature hippocampal granule cells. a,** Postsynaptic response of a young GC to electrical stimulation of ML and GCL GABAergic and glutamatergic inputs in the absence of blockers (n=7). V_{hold} = -80 mV. (i) Subthreshold EPSP induced by a double pulse in the ML (100 Hz, 200 µs, 29.0±5.6 µA, red). (ii) GPSP evoked by GCL burst stimulation at low intensity (8 at 50Hz, 200 µs, 5.6±0.5 µA, blue) boost AP firing. (iii) A 3-fold increase in GCL stimulation intensity inhibited AP generation (16.8±1.6 µA). (iv) GCL-evoked GPSPs are fully blocked by gabazine, whereas ML-evoked EPSPs are sensitive to both, gabazine and NBQX plus AP5.

This bidirectional response behavior of AP generation and inhibition was also observable in whole-cell recordings using a pipette solution with chloride ion concentration adapted to physiological values (Figure 10). Moderate stimulation of ML fibers (29.0±5.6 µA) induced AP firing in ~50% of DCX^+ young granule cells (n=4 of 7 spiking GCs). However, in most cases stimulation failed to induce action potentials, resulting in an overall firing probability of 18.6±7.7% (n=7, Figure 10a(i), c). GCL stimulation (5.6±0.5 µA) induced spiking in only one cell but effectively boosted AP firing when combined with ML inputs to an AP firing probability of 90±3.8% (n=7, Figure 10a(ii), c). In contrast, strong GABAergic synaptic stimulation (16.8±1.6 µA) increased depolarization but completely blocked subsequent AP generation (Figure 10a(iii), c). AP firing was strongly dependent on GABAergic synapses, since it was fully blocked by gabazine (Figure 10a(iv)). Whereas GCL stimulation evoked only GABAergic synaptic inputs, a small contribution of glutamatergic synapses was found to be activated by ML stimulation with an amplitude of 13.2±6.5 mV (n=6, Figure 10a(iv)). Glutamatergic ML inputs alone never induced firing in DCX^+ young granule cells (n=6), consistent with the absence of dendritic spines and the small glutamatergic synaptic currents at this developmental stage (Zhao et al. 2006, Ge et al. 2006, Mongiat et al. 2009).

Figure 10 (continued) **b,** Postsynaptic response of a young GC to electrical stimulation of ML and GCL GABAergic inputs in the presence of 10 µM NBQX and 25 µM AP5 (n=12-15). V_{hold} = -80 mV. (i) Subthreshold GPSP induced by a double pulse in the ML (100 Hz, 200 µs, 33.7±3.5 µA, red). (ii) GPSP burst (8 at 50Hz, 200 µs, 7.7±0.9 µA, blue) evoked by GCL stimulation boost AP firing. (iii) Strong GCL stimulation inhibited AP generation (20.9±3.5 µA). (iv) ML and GCL GPSPs are fully blocked by 10 µM gabazine. **c, d,** Firing probability in different conditions showing that pairing of ML and GCL stimulation pushed more effectively AP generation in young granule cells than either stimulation alone in the absence (**c**) or presence of glutamatergic blockers (**d**).

Thus, GABAergic inputs effectively controled spiking of young granule cells under physiological conditions. But are GABAergic synapses able to drive AP firing in the absence of additional glutamatergic input? Whole-cell recordings of GABAergic postsynaptic potentials (GPSPs) in the presence of glutamatergic blockers show that the stimulation of ML interneurons (33.7±3.5 µA) usually induces APs with a low probability of 27.3±10.7% (n=15, Figure 10b(i), d). GABAergic inputs recruited by GCL burst stimulation (7.7±0.9 µA) in general did not evoke APs (n=2 of 15 spiking cells, average AP probability of 4.0±2.9% (n=15); Figure 10d). Using the paired protocol with subsequent GCL and ML stimulation, GABAergic synaptic inputs reliably elicited AP firing (in n=15 of 15 cells with AP probability of 90.7±3.3%, Figure 10b(ii), d). As in physiological saline, a 3-fold increase in GCL stimulation intensity (ML-GCL pairing high, 20.9±3.5 µA) completely inhibited subsequent AP induction (n=12, Figure 10b(iii), d). Both, ML and GCL inputs rely on $GABA_A$ receptor containing synapses as they were fully blocked by 10 µM gabazine (n=5, Figure 10c(iv)). These data show that GABAergic inputs are sufficient to evoke APs in young GCs. However, GABAergic generation of APs is restricted to low stimulation intensities.

The contribution of glutamate to AP generation seemed to be rather small, as the firing probabilities were not decreased in the presence of glutamate blockers (Figures 9b, 10c and d). However, glutamatergic synaptic inputs had an effect on the timing of AP induction and enabled AP discharge at short latency (Figure 11). Spikes mediated only by GABA occur with a long delay. A strong increase of AP firing conspicuously occurs 17 ms after ML stimulation onset with only 2.8% of APs generated earlier (average delay 25.7±1.2 ms, n=15 cells, Figure 11b, d). In the population of spikes mediated by GABA and glutamate together, a substantial proportion was generated earlier than 17 ms (40.5%) with a mean delay of 21.6±2.7 ms (n=7 cells, Figure 11a, c, d). Furthermore, about 20% of the spikes generated in physiological saline occur within the first 10 ms and thus before the second ML stimulus was applied (18.9%, n=7 cells, Figure 11d). These results together indicate that a single stimulation of glutamatergic fibers is sufficient to induce spiking subsequent to GABAergic depolarization.

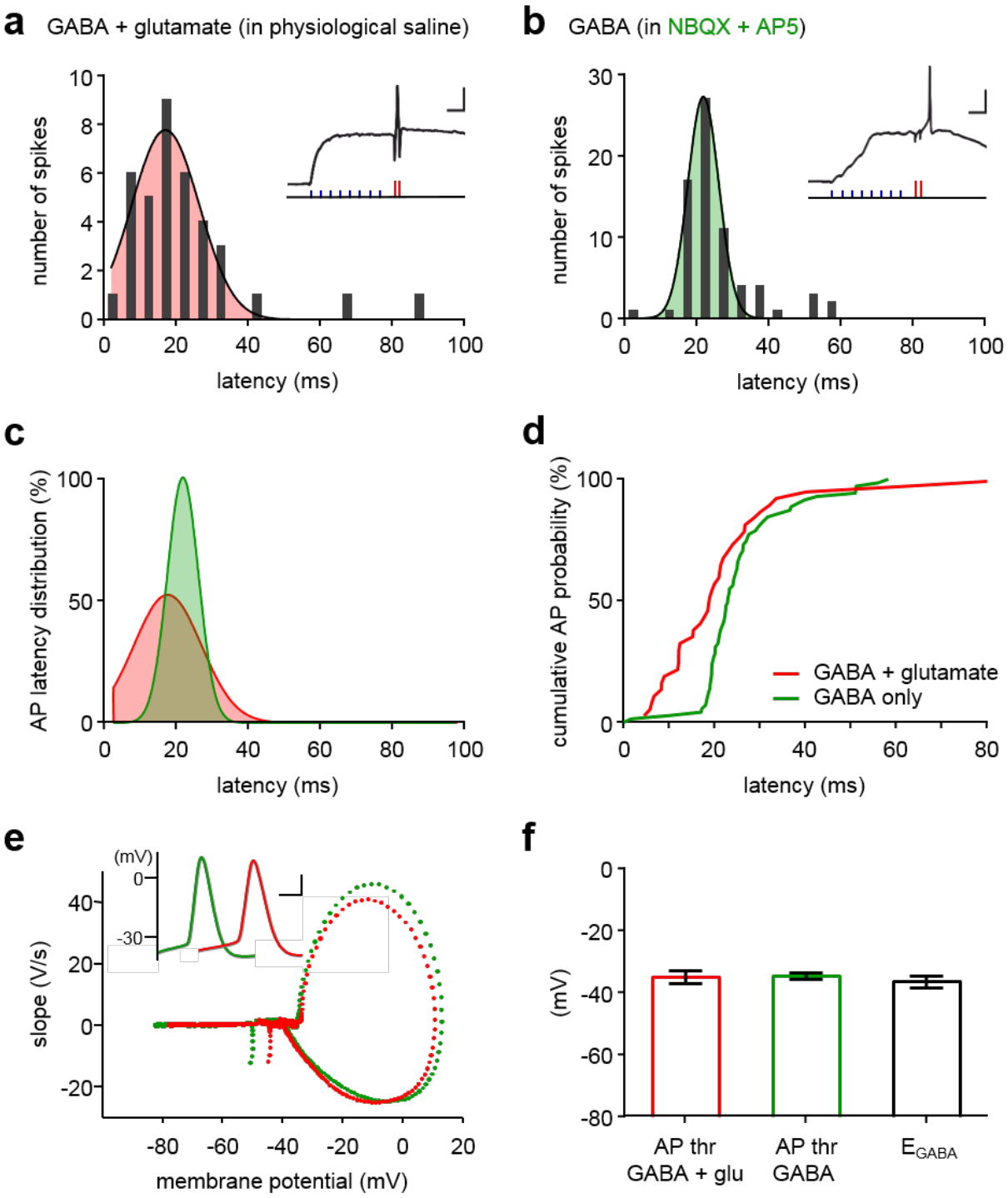

Figure 11 **AP firing enabled by glutamatergic inputs at short latency with a threshold similar to E_{GABA}. a,** Numbers of spikes elicited by GABAergic and glutamatergic inputs at different latencies after ML-stimulation onset. Data were fitted with a Gaussian distribution. Inset: Representative trace of AP firing induced by combined GCL- and ML-stimulation from a holding potential of -80mV. Stimulation protocol same as in Figure 6c(ii) with low GCL burst stimulation (blue) followed by ML stimulation (red). Scale 20pA, 40 ms. **b,** Same as **a** for inputs mediated only by GABA. **c,** Overlay of Gaussian distributions of GABA + glutamate (red) and GABA-only (green) APs normalized to the integral. **d,** Cumulative distribution of AP latencies.

The action potential threshold was detected from phase plots of APs elicited only by GABA or in the combination with glutamate (Figure 11e, -34.9±1.0 mV, n=9 and -35.1±2.2 mV, n=4, respectively). Figure 11f shows that the AP threshold does not differ in these two settings. Furthermore, the AP threshold is similar to the GABA reversal potential (-36.7±1.9 mV, n=10, P=0.8634, Kruskal-Wallis test), which might contribute to an efficient GABAergic control of AP firing.

Taken together, these experiments demonstrate a bidirectional control of action potential generation by GABAergic inputs. Low GABAergic synaptic transmission can induce AP firing, either alone or by boosting subthreshold glutamatergic EPSPs. By contrast, strong GABAergic inputs effectively block action potentials in newly generated young granule cells.

However, the generation of action potentials might be dependent on both, the timing of converging inputs as well as the synaptic strength of the underlying conductances. Therefore, these two parameters were gradually altered in the following experiments in order to investigate their corresponding impact on AP firing in young hippocampal granule cells.

Figure 11 (continued) **e,** Phase plot of APs generated by synaptic stimulation in physiological saline (red) and in the presence of glutamatergic blockers (green). Inset: AP traces used for phase plots. Gray, original data. Color, after smoothing with a Savitzky-Golay filter (2nd order, 1 ms window width). Scale, 10mV, 2.5 ms. **f,** Threshold (thr) of APs evoked either by GABAergic and glutamatergic synaptic inputs or by GABA alone is similar to E_{GABA} (n = 4, 9 and 10, respectively, P=0.8634, Kruskal-Wallis test).

4.4 Efficient temporal integration of EPSPs and GPSPs in young granule cells

As a first approach, the dependence of the relative timing of GABAergic and glutamatergic PSPs on AP firing was investigated. Glutamatergic EPSPs were replaced by small postsynaptic depolarizations evoked by somatic current injections (25.7±0.6 mV, n=12). These mock EPSPs were combined with the activation of perisomatic GPSPs using GCL stimulation in the presence of NBQX and AP5 (Figure 12). First, the mock EPSP was shifted in time relative to GCL burst stimulation of 8 stimuli (50 Hz, 200µs) using a moderate intensity of 10 µA (Figure 12a, b). Action potentials were elicited over a broad time window with more than 50% AP probability for 349.0±12.1 ms (n=12, Figure 12c). Notably, coincident application of a mock EPSP with GPSP stimulation (second trace in Figure 12b) reliably induced AP firing, when GABA-conductance (g_{GABA}) reached 78.6% of its peak (1.05±0.27 nS, n=12).

In order to mechanistically understand the temporal integration of synaptic inputs in young GCs, mock EPSPs (23.3±0.4 mV, n=13) were combined with 2 short pulses in the GCL (2 stimuli at 50 Hz, 50 µA, 200 ms, Figure 12d-e). Spike doublets are also typical firing patterns of presynaptic parvalbumin expressing basket cells (Klausberger et al. 2003, Fuentealba et al. 2010). Due to the slow membrane time constant of the young GCs (τ_m = 124.6±14.0 ms, n=13), GABA-mediated depolarization considerably outlasted the underlying PSC. The average AP probabilities were fitted with a sigmoidal rise and decay (see methods, equation 2) and revealed an efficient temporal integration with a firing probability above 50% for almost 200 ms (Δt = 184.21±3.35 ms, n=13, Figure 12f), with a linear dependence of Δt on τ_m (slope = 0.94±0.51, R^2 = 0.33). This indicates that young cells with slow membrane time constants efficiently integrate synaptic inputs over time, whereas this temporal integration sharpens with cell maturation and concomitant decrease of τ_m.

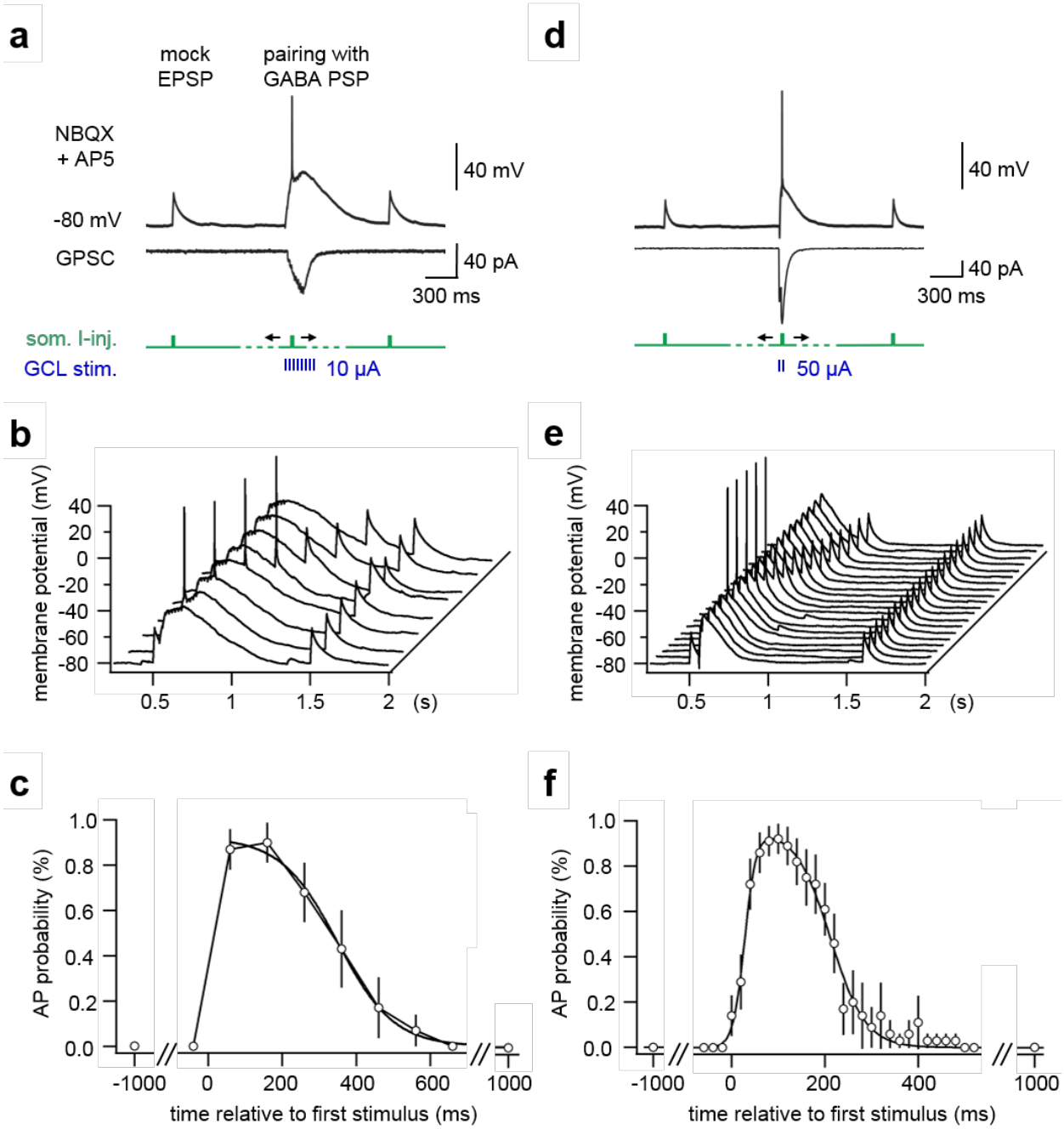

Figure 12 **Efficient temporal integration of EPSPs and GPSPs. a,** Mock EPSPs with an amplitude of ~25 mV were generated by a somatic current injection (10 ms, green) and paired with GPSPs evoked by GCL burst stimulation (8 times at 50 Hz, 10µA, 200 µs, blue) in the presence of NBQX and AP5 (upper trace). Mock EPSP was shifted in time relative to GPSP stimulation in steps of 100 ms. GABAergic postsynaptic currents (GPSC) were stimulated using the same intensity. **b,** A sequence of traces showing pairing with mock EPSP at increasing delays to onset of GCL stimulation. Firing occurred when mock EPSP was applied simultaneously with GPSP (second trace). **c,** AP probability is plotted against mock EPSP delay relative to first stimulus of GCL burst (n=12). Decay slope was fitted with a sigmoidal function. **d,** Mock EPSP was paired with GCL double pulse stimulation (2 times at 50 Hz, -50µA, 200 µs) and shifted in small steps of 20 ms. **e,** Similar to **b** with protocol shown in **d**. **f,** Similar to **c** with protocol shown in **d** (n=13). Data were fitted with the product of two sigmoidal functions.

To test whether GABAergic depolarization can boost AP firing also in mature GCs as claimed in a computational modeling study (Chiang et al. 2012), a mock EPSP (22.0±0.5 mV, n=13) was combined with GPSPs elicited by GCL stimulation in the presence of NBQX and AP5 in mature GCs (Figure 13a). The mock EPSP was shifted in time relative to GCL stimulation (2 stimuli at 50 Hz, 50 µA, 200 ms). Although GABAergic inputs generated a depolarization of 3.3±0.5 mV in mature granule cells, coincidentally applied mock EPSPs were always reduced in amplitude to, on average, 87.9±2.0% of control (n=13, Figure 13b). Whereas the reduction of PSP amplitude is restricted to the time of active GABA conductance, a small increase in total amplitude by 5.0±1.2% was reached 80 ms after the last stimulus.

The analysis of subthreshold events in newborn granule cells stimulated with the same protocol revealed that the total amplitude of mock EPSPs paired with GPSPs is never reduced but increased to up to 238.2±3.0% of control (Figure 13c, d). Thus, perisomatic synaptic inputs induce a precisely timed GABAergic inhibition in mature hippocampal granule cells but exclusively provide depolarization to newly generated neurons.

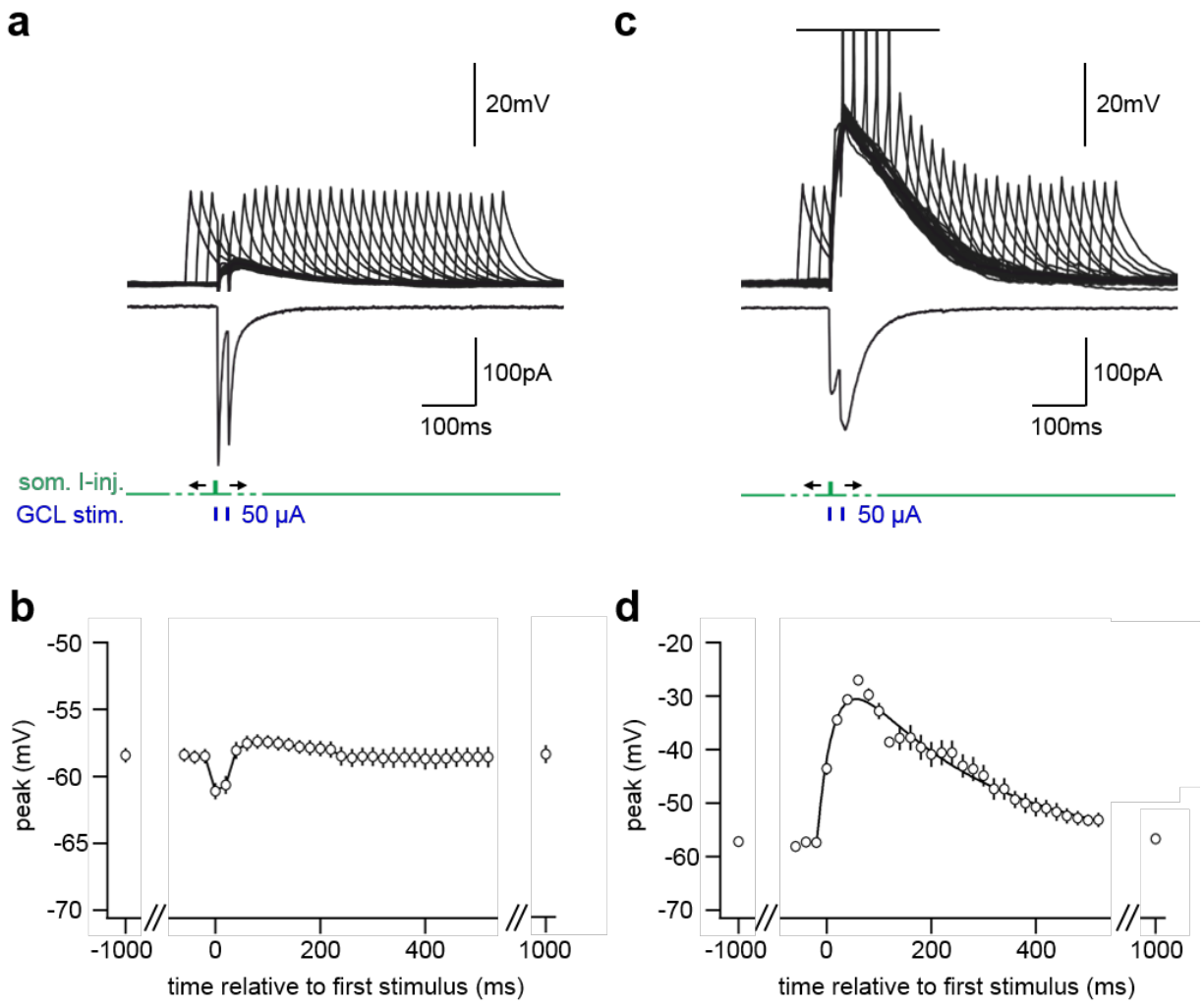

Figure 13 **Precise timing of GABAergic inhibition in mature neurons. a,** Combined somatic current injection (green) and extracellular GCL stimulation (50 µA, 200 µs, blue) in a mature GC in the presence of NBQX, AP5 and CGP. Mock PSP (22.0±0.5 mV, n=13) was shifted relative to GABA conductance. **b,** Summary plot of PSP peak potentials at different delays relative to first stimulus. Reduction of PSP peak potential is restricted to GABAergic conductance (n=13). **c,** Combined somatic current injection and extracellular GCL stimulation in a young GC in the presence of NBQX, AP5 and CGP. Mock PSP (23.3±0.4 mV, n=13) was shifted relative to GABA conductance. APs were cut for better illustration of failure PSPs. **d,** Summary plot of failure PSP peak potentials at different delays relative to first stimulus fitted with (n=13).

4.5 Dynamic regulation of GABAergic AP facilitation

To further understand the impact of the GABAergic synaptic strength on facilitation and inhibition of AP firing, a postsynaptic mock EPSP was combined with GCL stimulation of different intensities in the presence of NBQX and AP5 (Figure 14). For mock EPSPs, somatic current injections (10 ms, 56.0±4.3 pA, range 35-80 pA) were adjusted to evoke a ~20-mV-depolarization (23.3±0.6 mV, n=10) when applied at a membrane potential of -80 mV. As shown in Figure 14a, increasing GABAergic synaptic activity can facilitate the generation of APs at intermediate stimulation intensities. To quantify this phenomenon, GABA PSCs were subsequently recorded in voltage clamp with the same stimulation intensities in the very same cells and the conductances were measured at the time of somatic current injection (Figure 14a, lower traces). The analysis revealed that the probability of AP firing is enhanced by GABAergic depolarization already with small conductances below 1 nS reaching a peak probability of 96±2% at 1.5±0.1 nS (n=10). Furthermore, the data could be fitted with a sigmoidal rise and decay (see methods, equation 2) showing that a high firing probability (> 50%) is restricted to a conductance window between 0.40±0.08 and 3.56±0.27 nS. With larger GABAergic activity, however, AP firing is effectively inhibited.

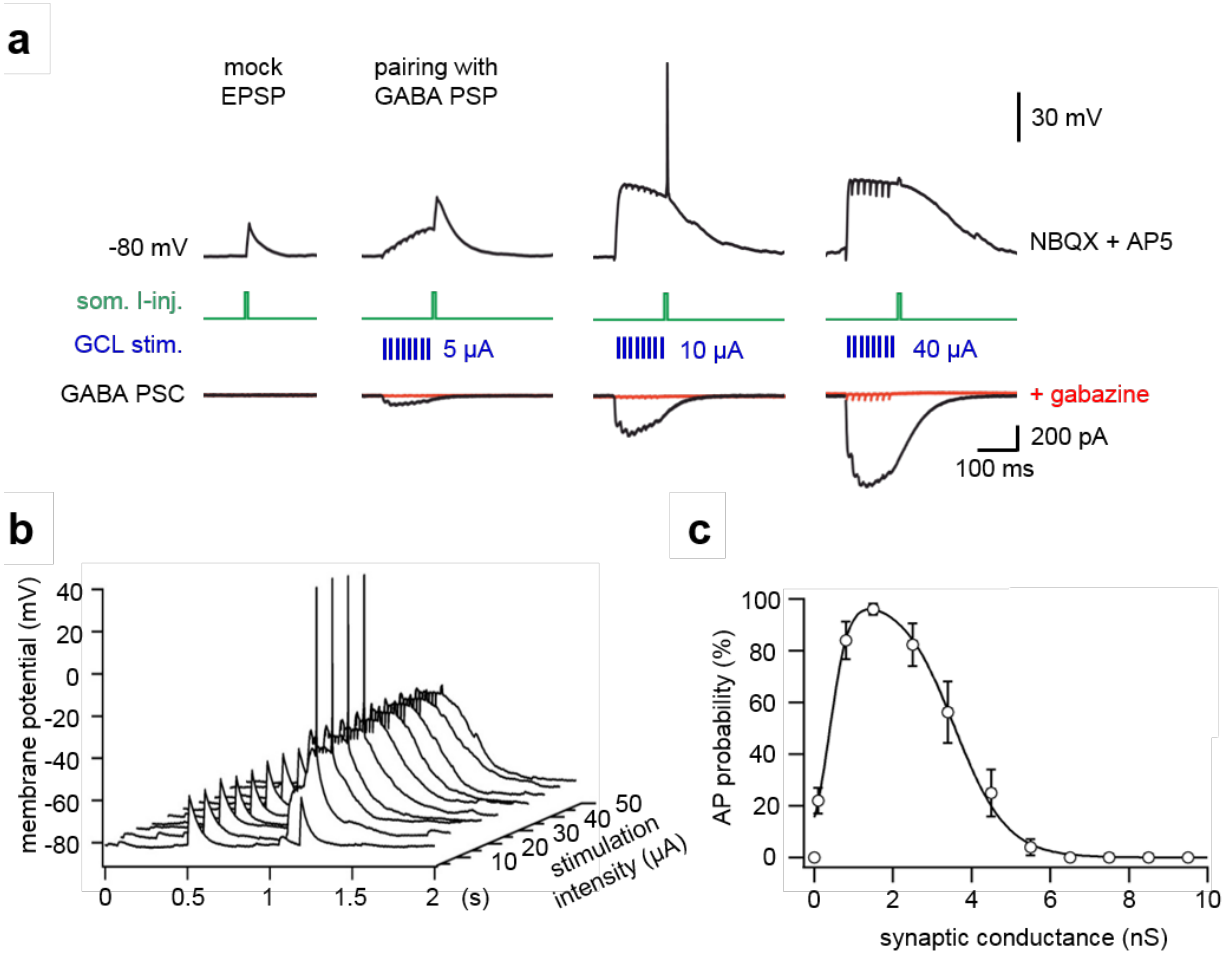

Figure 14 **GABA-induced excitation and inhibition of AP firing. a,** Mock EPSPs were generated by a somatic current injection (10 ms, green) and paired with GPSPs evoked by stimulation pulses of increasing intensity (200 µs, 8 times at 50 Hz) in the presence of NBQX and AP5 (upper traces). Lower traces show GABAergic synaptic currents (GPSC) using the same stimulation intensity before (black) and after application of gabazine (red). **b**, A sequence of traces showing pairing with increasing synaptic stimulation intensity as indicated on the right axis. **c**, Firing probability is plotted against the GPSC conductance, showing that firing could only be evoked within in certain conductance range (0.40-3.56 nS, n=10). Continuous line represents a fitted curve consisting of the product of a sigmoidal rise and decay.

What is the reason for the inhibition of AP firing? As a first step to understand the underlying mechanisms, mock EPSPs were compared before and during the evoked GPSPs when the mock EPSP failed to induce AP firing (Figure 15a). The amplitude of the mock EPSP was strongly reduced during large GPSPs that inhibited AP firing (23.3±0.6 mV versus 7.3±0.9 mV, n=10; P=0.0020, Wilcoxon signed rank test; Figure 15b). Similarly, the decay time course of the mock EPSP (τ = 120.7±19.4 ms) and the duration measured at half-maximal amplitude (half width = 96.1±16.9 ms) were strongly decreased to 3.4±0.8% and 12.2±2.1% of control, respectively (both, n=10; P=0.0020, Wilcoxon signed rank test; Figure 15b). The reduction in mock EPSP amplitude and the faster decay indicates that the conductance activated by GABAergic synapses generates a membrane leak conductance, which can effectively shunt further depolarization of the membrane.

To test this hypothesis more quantitatively, the mock EPSP parameters for all subthreshold responses were analyzed over the full range of GABAergic synaptic conductances (Figure 15c-e). As the newly generated young neurons show a high electrical input resistance (R_{in} ≈ 4 GΩ) and a small membrane capacitance (Cm ≈ 20 pF) indicating a small and compact cell morphology, a single compartment model was used to quantitatively predict the effect of a synaptic conductance onto the measured mock EPSP parameters (Figure 15c-e, see methods). Remarkably, this simple model (dashed lines) quantitatively predicted the decrease of the mock EPSP decay time constant with increasing GABAergic conductance (Figure 15c). Furthermore, the data were fitted with an analytical function describing the single compartment model with a scaled GABAergic synaptic conductance as a free parameter (equation 3, Figure 15c, solid line). The similarity of the fitted curve to the theoretical model prediction strongly supports the conclusion that the mock EPSP is reduced by the GABAergic synaptic conductance via shunting inhibition. Similarly, the model also predicted the decrease in mock EPSP amplitude (Figure 15d, equation 6) and the reduction of the half duration (Figure 15e, equation 12). On average, fitting the three different parameters revealed a scaling factor of 1.02±0.19, indicating that the experimentally measured GPSC conductance was similar to the predicted shunting conductance associated with the decreased membrane time constant and the decreased input resistance (Figure 15c-e, solid lines). This analysis shows that shunting inhibition is sufficient to fully explain the reduction in excitability with increasing GABAergic synaptic activity.

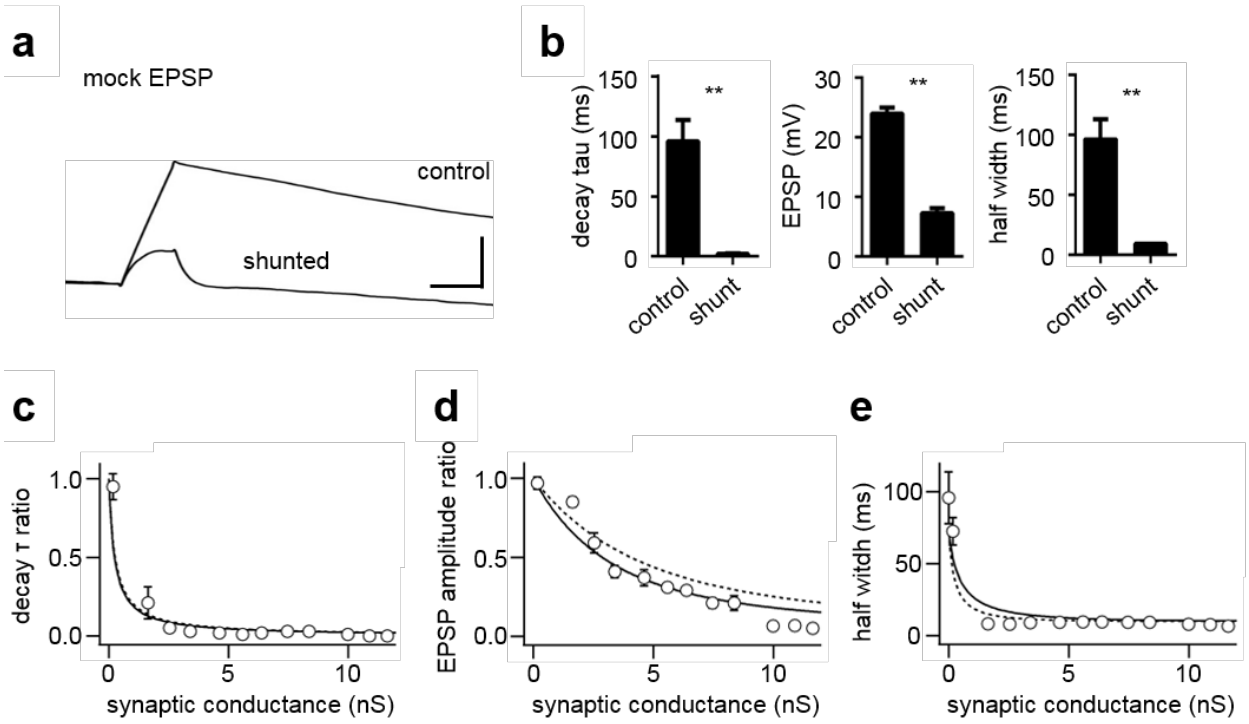

Figure 15 **High GABAergic activity generates powerful shunting inhibition. a,** Overlay of the mock EPSPs before and after strong GPSP stimulation. Scale, 10 mV, 10 ms. **b,** Summary graphs of decay time constant, EPSP amplitude and half width comparing the mock EPSP before (control) and during (shunt) the evoked GPSPs at the smallest synaptic conductance where AP generation was completely inhibited (all: n=10, P=0.0020, Wilcoxon matched-pairs signed rank test, W=55.00). **c-e,** The relative decrease of shunted mock EPSP decay time constant (**c**) and amplitude (**d**) and the half duration (**e**) are plotted against GPSC conductance (n=10). Dotted lines represent theoretically predicted curves assuming a homogenous spatial distribution of synaptic shunt conductances. Continuous lines represent curves fitted to the data with a scaled shunt conductance as a free parameter (see methods).

Although the experiments outlined above indicate that GABA-receptor mediated shunting inhibition is sufficient to explain the restriction of AP firing, other additional inhibitory mechanisms could contribute to this phenomenon. However, if this simplified model is correct, it should be possible to compensate a partial reduction of GABA conductance by increased synaptic transmission. To address this question, a low concentration of the $GABA_A$-receptor antagonist gabazine (0.2 µM) was applied, which blocked GPSCs to 50.1±3.3% of control (n=8, Figure 16). Blocking half of the $GABA_A$ receptors efficiently shifted GABAergic excitation towards larger stimulation intensities and strongly reduced shunting inhibition (Figure 16b). The cumulative probability for AP firing at 50% is shifted by a factor of ~2 (from 0.31 to 0.63 of maximal stimulation intensity, n=8, Figure 16d) indicating that recruitment of 2-times more synapses by larger stimulation intensity is sufficient to compensate for the 50% decrease in $GABA_A$ receptor conductance per synapse. This linear compensation mechanism argues against a differential recruitment of further voltage-dependent conductances or different populations of excitatory and inhibitory interneurons by different stimulation intensities. By contrast, these results suggest that shunting of mock EPSPs by $GABA_A$-receptors effectively inhibits AP generation at high stimulation intensities. Larger concentrations of gabazine (10 µM) fully blocked GPSPs and AP firing (Figure 16c, d), showing that both, GABAergic excitation and inhibition is dependent on the activation of $GABA_A$ receptors.

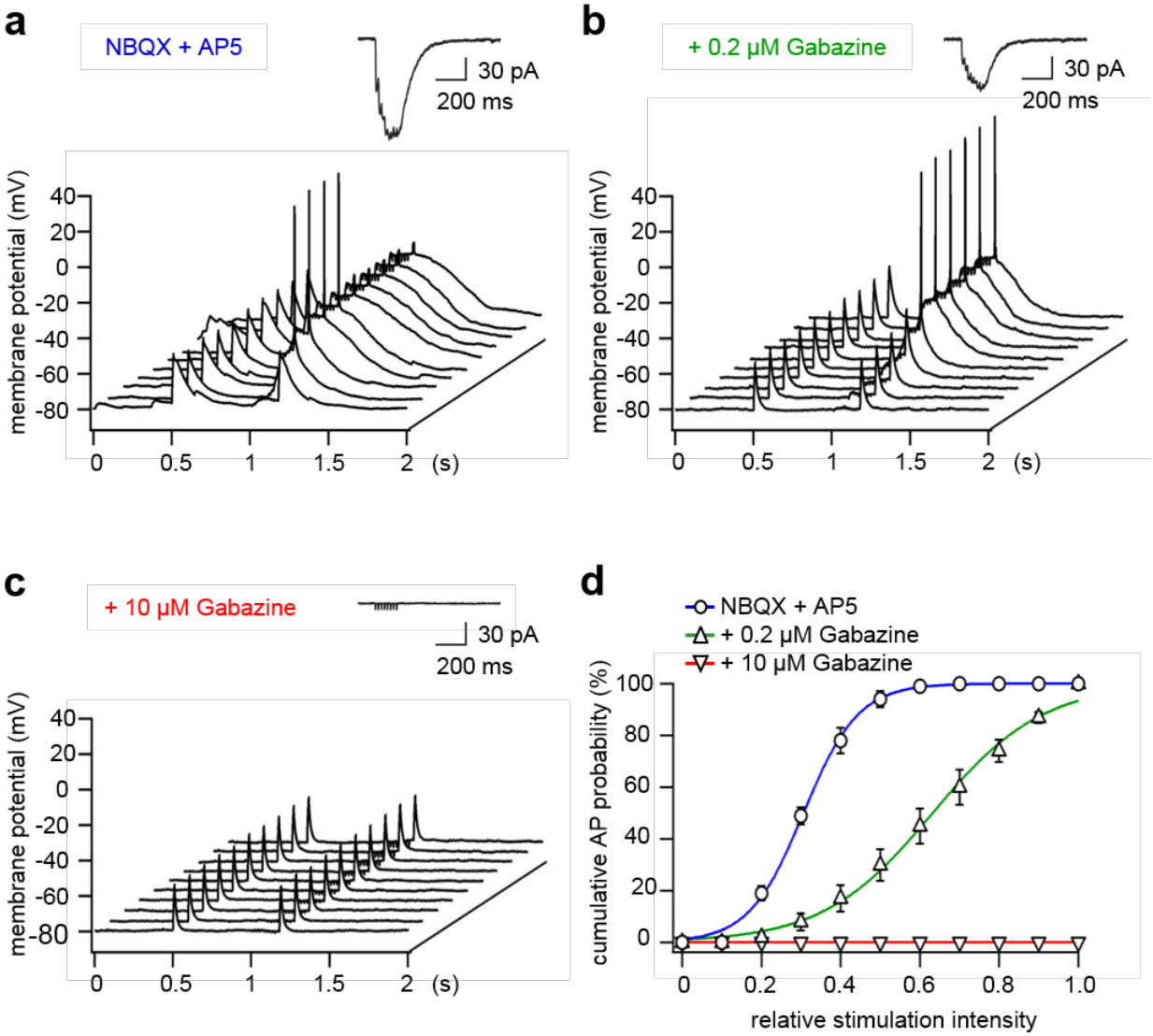

Figure 16 **Dynamic shift from GABAergic excitation to shunting inhibition. a**, A sequence of traces showing mock EPSPs followed by pairing with increasing GABAergic synaptic conductances in the presence of NBQX and AP5. Inset, corresponding GPSC. **b**, Additional application of low concentrations of gabazine (0.2 µM) shifted AP firing towards stronger stimulation intensities, indicating that shunting is mediated by $GABA_A$-receptors. Inset, GPSC conductance is reduced to ~50%. **c**, Application of 10 µM gabazine fully blocked GPSPs showing that both, GABAergic excitation and inhibition is dependent on the activation of $GABA_A$-receptors. Inset, GPSC is fully blocked by gabazine. **d**, Summary plot showing the cumulative AP probability with increasing stimulation intensity in control and after application of 0.2 and 10 µM gabazine (n=8).

5 Discussion

This study demonstrates for the first time that synaptic GABAergic transmission onto newly generated DCX^+ granule cells of the adult hippocampus can induce action potential firing. Within 2 to 3 weeks after mitosis, E_{GABA} is constantly depolarized to about -35 mV, but drops rapidly close to resting potential parallel to the loss of doublecortin expression. GABAergic synaptic transmission to DCX^+ young granule cells enables action potential generation over a long time window of ~200 ms and furthermore bidirectionally controls AP firing dependent on the strength of $GABA_A$-receptor conductance. Action potential firing is maximal at low synaptic activity (~0.5-3.5 nS) and blocked via shunting inhibition at large synaptic strength. Therefore, GABAergic interneurons can facilitate or inhibit AP firing in newly generated young granule cells dependent on their specific activity pattern. This might contribute to dynamic regulation of granule cell maturation and survival.

5.1 GABAergic switch from depolarization to hyperpolarization

One open question that has not been elucidated so far is the timing when GABAergic synaptic inputs switch from depolarization to hyperpolarization in adult-born neurons (Pallotto and Deprez 2014). Consistent with previous reports, the present study shows a reversal potential of GABA receptors more positive than the resting potential in newly generated granule cells of the adult hippocampus ($E_{GABA} \approx$ -35 mV, Ge et al. 2006, Karten et al. 2006, Chancey et al. 2013). In addition, the results reveal that elevated E_{GABA} levels strongly correlate with the input resistances of granule cells. The sudden drop of E_{GABA} indicates that the intracellular chloride concentration is not continuously down regulated but heavily dependent on the maturational state of the single cell. This is in contrast to the hypothesis of a continuous maturation (Ge et al. 2006), as it was recently reported also for spine generation and input integration properties of immature granule cells (Piatti et al. 2011, Brunner et al. 2014).

Furthermore, E_{GABA} levels correlate with the expression of DCX, a microtubule associated protein important for cell migration as well as axonal and dendritic outgrowth. The signaling pathways regulating morphological development,

proliferation and survival were shown to be mediated by the cAMP response element-binding protein CREB (Jagasia et al. 2009, Magill et al. 2011). CREB phosphorylation and hence activation depends on GABA-mediated depolarization, as loss-of-function experiments for CREB as well as NKCC1 result in impairment of morphological maturation and cell survival (Jagasia et al. 2009). Interestingly, CREB phosphorylation is restricted to the developmental period of high DCX expression and is downregulated as newly generated granule cells loose DCX and initiate the expression of the mature granule cell marker calbindin (Jagasia et al. 2009), consistent with the hypothesis that depolarizing GABA is restricted to the endurance of DCX expression. This indicates that E_{GABA} remains high as long as newborn neurons underlie high levels of structural and functional modifications and quickly decreases afterwards.

5.2 AP firing in newly generated granule cells of early postnatal development and adulthood

During embryonic and early postnatal development, when excitatory glutamatergic circuits are not yet functional, GABA can act as an excitatory transmitter due to a depolarized $GABA_A$-reversal potential (Owens et al. 1996, Ben-Ari et al. 1997, Leinekugel et al. 1997, Gao and van den Pol 2001, Valeeva 2010). Activation of $GABA_A$ receptors can therefore lead to giant depolarizing potentials (GDPs) and the initiation of action potential underlying early network oscillations, which are coordinated by local GABAergic interneurons (Ben-Ari et al. 1989, 2007, Garaschuk et al. 1998, 2000, Wang et al. 2001, Ben-Ari 2002, Tyzio et al. 2007). Thereby, GABA supports activity-dependent growth of dendrites and synapses, important for proper brain development (Wang and Kriegstein 2011). Although neonatal brains are known to be highly susceptible to epileptic seizures, the neurons are relatively resistant to damages induced by seizures or anoxic episodes compared to the mature brain (Nardou et al. 2013). Factors that form a protective environment include a lower density of active synapses, high concentrations of BDNF and reduced levels of cytokines associated with seizures (Tandon et al. 1999, Rizzi et al. 2003).

During adult neurogenesis, cell maturation is recapitulating the ontogenic development with a depolarizing GABA due to high expression of NKCC1 within the first weeks post-mitosis (Ben-Ari 2002, Owens and Kriegstein 2002, Payne et al. 2003). In contrast to post-natally born neurons, GC generated in the adult brain are born into

a mature environment with a high density of GABAergic and glutamatergic synapses, which release transmitters not only in the synaptic cleft but also produce a substantial amount of spillover. Furthermore, cholinergic, dopaminergic, serotonergic, vasopressin and oxytocin projections from other brain regions innervate the dentate gyrus and may influence hippocampal neurogenesis (Veena et al. 2011, Strange et al. 2014). The young granule cells however show enhanced electrical excitability but a lower Ca^{2+}-buffer capacity than mature granule cells and large AP-evoked dendritic Ca^{2+}-transients (Stocca et al. 2008). As both, glutamate and GABA are depolarizing in the young neurons, a mechanism to protect the young cells from over excitation and Ca^{2+}-dependent apoptosis during strong network activity is mandatory. Therefore, GABAergic excitation has to be regulated much more precisely as GABA has to serve as both, a trophic factor and an inhibitory transmitter to avoid excitotoxicity of the young neurons. Thus, under which circumstances are APs elicited in newly generated young granule cells of the adult hippocampus?

In general, adult-born granule cells are able to fire sodium-dependent action potentials in response to somatic current injection very early after birth. Esposito et al. (2005) reported sodium-mediated action potential generation already within the first week post-mitosis. Own observations show both, calcium- and sodium-spikes in DCX-expressing granule cells with high R_{in} (>50 GΩ) and thus most likely very young neurons (data not shown). Whether APs can be induced by synaptic inputs was elucidated by the present study.

The results demonstrate that brief bursts of small GPSPs effectively induce AP firing by boosting small glutamatergic EPSPs or even spatially distributed GPSPs (Figure 10a(ii) and b(ii)). The latter might be of particular importance in the early cell development, when the young neurons receive only GABAergic synaptic inputs. The fact that the AP threshold equals E_{GABA} may represent the basis for an efficient control of AP generation. Low GABAergic transmission powerfully depolarizes the young neurons to be ready to respond to small EPSPs, whereas large $GABA_A$-conductances effectively shunt subsequent AP-firing. Interestingly, even short GPSPs provide a long lasting depolarization due to the slow membrane time constant and promote action potential generation over a broad time window of ~200 ms (Figure 12). That interval corresponds to theta cycle activity of 4-8 Hz prominent in the hippocampal field potential during spatial exploration (Soltesz et al. 1993, Ylinen et al. 1995). This implies

that single small EPSPs from the entorhinal cortex, which predominantly occur during hippocampal theta firing (Pernía-Andrade and Jonas 2014), can therefore very efficiently excite young granule cells. The large GABAergic depolarizations that boost EPSPs are regulated by E_{GABA}, which is ~-35 mV in young neurons due to an elevated internal chloride concentration. With progressive maturation and concomitant hyper-polarization of E_{GABA}, larger glutamatergic EPSPs will be necessary to induce AP firing in a granule cell. After full maturation, GABAergic synaptic inputs provide a profound shunting inhibition.

A previous study that used computational modeling claimed that AP firing is facilitated by GABAergic synaptic inputs also in mature hippocampal granule cells (Chiang et al. 2012). Though E_{GABA} is close to resting membrane potential, it is slightly more depolarized and may boost subthreshold EPSPs dependent on the location of the GABA synapses and the relative timing of EPSP and GPSP. They showed, that dendritic GPSPs provide a small somatic depolarization, which, when applied preceding to near-threshold EPSPs, induces AP firing. However, neither somatic nor coincidently activated dendritic GPSPs were able to elicit APs in mature granule cells. Our experimental results confirm the modeling of Chiang et al. (2012). Similar results were also demonstrated for mature cortical pyramidal cells where coincident EPSPs and somatic GPSPs never resulted in AP firing (Gulledge and Stuart 2003). In stark contrast to these findings, our results show that in newly generated young granule cells GABAergic inputs can effectively boost AP firing when EPSPs were initiated coincidentally with active GABA conductances.

Together, these results demonstrate that during low network activity with small GABAergic PSPs elicited in young GCs, converging inputs are efficiently integrated over time. However, a dense network of GABAergic interneurons provides intense lateral inhibition along the granule cell layer. Strong GABAergic transmission as it might occur during high network activity induces shunting inhibition in the young GCs and thereby effectively blocks AP generation at conductances above ~3.5 nS. This bidirectional GABAergic control of AP firing therefore enables the integration of newly generated neurons but at the same time provides a reliable protection from activity induced excitotoxicity.

5.3 Dynamic shift from GABAergic excitation to shunting inhibition

There is a large number of different types of interneurons in the hippocampus (Freund and Buzsaki 1996) and it was suggested that the young neurons gradually form GABAergic synaptic connections during post-mitotic maturation similar to the preexisting neurons during embryonic and postnatal development (Esposito et al. 2005). GABAergic input to adult-born young granule cells is provided by a variety of hippocampal interneurons located in the subgranular zone (parvalbumin (PV)-expressing basket cells and hilar commissural-associational pathway-related (HICAP) cells), hilus (hilar perforant path-associated (HIPP) and somatostatin (SST)-expressing interneurons), and molecular layer (neuropeptide Y (NPY)-expressing Ivy/ neurogliaform neurons, molecular layer perforant path-associated (MOPP) and axo-axonic cells), shown by several recent studies using monosynaptic rabies virus-based tracing techniques (Deshpande et al. 2013, Vivar et al. 2013, Bergami et al. 2015). Especially PV^+ basket cells seem to innervate newborn granule cells in an early developmental phase within the first week after mitosis (Deshpande et al. 2013, Song et al. 2013).

But how many of these interneurons are necessary to enable GABAergic excitation in young granule cells? Using paired patch-clamp recordings, it was shown that one of the first GABAergic synaptic inputs onto newborn cells formed by NPY-positive neurogliaform cells generate relatively small unitary synaptic conductances of 0.21 nS (Markwardt et al. 2011). Similarly, the here presented data show a small minimal conductance of 0.28±0.06 nS (n=10). Taking into account an average burst facilitation of ~160%, a unitary burst conductance of 0.28-0.45 nS would indicate that burst firing of only ~2 interneurons is sufficient to depolarize the young neurons close to E_{GABA} enabling a firing probability of more than 50% with coincident small subthreshold glutamatergic synaptic inputs (Figure 14c). Thus, the presented results indicate that GABAergic synapses enable AP firing initiated by small glutamatergic EPSPs during low and moderate hippocampal network activity. Furthermore, GABAergic interneurons can powerfully inhibit AP firing during strong network activity by shunting inhibition, although the reversal potential is strongly depolarized. The results indicate that there is a large number of interneurons connected to the young cells as the synaptic conductance could be strongly increased with higher stimulation intensity (up to 15 nS). Thus, during stronger network activity, when more than 25% of the interneurons are active (~4 nS), AP firing in young neurons can be effectively inhibited to protect newly generated young granule cells from over excitation.

The large number of presynaptic GABAergic interneurons might rise the hypothesis that the used stimulation intensities activated discrete subpopulations of interneurons that are responsible either for the excitatory or inhibitory impact on the young granule cells. However, the results show that GABAergic excitation shifts towards 2-times higher stimulation intensities when the number of open $GABA_A$ channels are reduced by 50%. This demonstrates that shunting inhibition can be directly converted into excitation by homogenously reducing GABA-conductances modulated by the very same presynaptic interneurons, indicating that there are no specific subpopulations of excitatory and inhibitory GABAergic interneurons.

5.4 Functional significance of synaptically evoked AP firing

Why should AP firing be important in young neurons? The integration into the dentate gyrus network is essential for the positive selection and maturation of newly generated granule cells. This can be implemented by *de-novo* formation of new synaptic connections, strengthening of existing synapses via the induction of long-term potentiation (LTP) or unsilencing of silent synapses.

Theta-burst stimulations of perforant-path evoked EPSPs were shown to trigger the induction of long-term potentiation (LTP) when paired with postsynaptic APs, which is dependent on the activation of NMDA receptors (Schmidt-Hieber et al. 2004, Ge et al. 2007b). By contrast, no LTP is induced without postsynaptic spiking (Schmidt-Hieber et al. 2004). This would be consistent with an important role for postsynaptic APs to relief voltage-dependent Mg^{2+} block of NMDA receptors.

Furthermore, young granule cells show a relatively large number of ‘silent synapses’ expressing only NMDA-receptors but no AMPA receptors (Chancey et al. 2013). These synapses could be unsilenced by the use of a pairing protocol with strong postsynaptic depolarizations to 0 mV. The unsilencing was dependent on activation of NMDA receptors, again arguing that strong depolarization as occurring during AP firing might be important for the relief of the Mg^{2+} block and the induction of synaptic plasticity in newborn neurons.

In addition to synaptic NMDA receptors, it is well known that extrasynaptic dendritic NMDA receptors are involved in the formation of new synapses during long-term potentiation (Engert and Bonhoeffer 1999, Maletic-Savatic et al. 1999). More recently, it was shown in cortical pyramidal cells from young rats that a small number of about

10 brief pulses of caged glutamate onto a dendritic shaft is sufficient to induce rapid growth of new spines. The induction was dependent on the activation of extrasynaptic NMDA receptors and Ca^{2+}-dependent PKA activation (Kwon and Sabatini 2011). The development of extrasynaptic ionotropic NMDA and AMPA receptors in young hippocampal granule cells was described in a recent study (Schmidt-Salzmann et al. 2014). In contrast to an initial low density of AMPA receptors, which increases over cell maturation, NMDA receptor density was shown to be similarly high throughout development. Furthermore, it was suggested that newly generated granule cells form new synapses with entorhinal boutons previously synapsing onto spines of preexisting mature granule cells in a competitive manner (Toni et al. 2007). Together with our new data, this would suggest that GABAergic depolarization facilitates AP generation and thereby the activation of NMDA receptors by coincident spillover of glutamate to support new synapse formation in an activity dependent and associative manner.

Moreover, maturation, differentiation and cell survival are dependent on Ca^{2+}-mediated signaling cascades and excitatory GABA is believed to control the tempo of activity-dependent growth and differentiation in young neurons in the adult brain (Gu and Spitzer 1995, Ge et al. 2007a, Lepski et al. 2013). For adult-born newly generated granule cells within the first 3 weeks post-mitosis it was shown that GABAergic depolarization activates Ca^{2+}-dependent proteins to regulate growth and gene expression (Wong and Ghosh 2002, Konur and Ghosh 2005, Spitzer 2006, Jagasia et al. 2009). Calcium-dependent dendritic growth in young neurons was demonstrated to be regulated by CaMKIV (calcium/calmodulin-dependent protein kinase IV)-modulated CREB-phosphorylation and the AKT-mTOR pathway (Redmond et al. 2002, Kim et al. 2012). T- and L-type calcium channels in the young neurons can mediate the voltage-dependent increase of intracellular calcium (Owens et al. 1996, Schmit-Hieber et al. 2004, Lee et al. 2012). Remarkably, the Ca^{2+} transients evoked by APs have a two-fold larger amplitude than transients evoked by low-threshold Ca^{2+}-spikes (Stocca et al. 2008). Consistently, pharmacological blockade and cell specific knock-down of NMDA receptors strongly interfere with survival and dendritic growth during the first to third week after birth (Tashiro et al. 2006, 2007, Tronel et al. 2010). Therefore, it is most likely that AP-dependent Ca^{2+}-influx are of major importance not only for synapse formation, but also for survival of newborn granule cells during a critical developmental period.

5.5 Conclusion

The presented data show for the first time synaptically evoked AP-firing in adult-born young hippocampal granule cells less than 3 weeks post-mitosis. Action potential generation is dependent on $GABA_A$-mediated synaptic activity and can be modulated either by GABA alone or in synergy with glutamatergic inputs. For the young GCs, several key features were identified including depolarized E_{GABA}, high input resistance and the activity of presynaptic interneurons, which altogether provide the basis for an activity dependent bidirectional GABAergic control of AP firing dependent on hippocampal network activity. These findings represent an important contribution to our understanding of mechanisms underlying first neuronal signaling in newly generated neurons of the adult hippocampus.

6 References

Aimone J.B., Deng W., and Gage F.H. (2010). Adult neurogenesis: integrating theories and separating functions. *Trends Cogn Sci*, 14(7):325–337.

Akaike N. and Harata N. (1994). Nystatin perforated patch recording and its applications to analyses of intracellular mechanisms. *Jpn J Physiol*, 44(5):433–473.

Altman J. (1962). Are new neurons formed in the brains of adult mammals? *Science*, 135(3509):1127–1128.

Altman J. (1963). Autoradiographic investigation of cell proliferation in the brains of rats and cats. *Anat Rec*, 145:573–591.

Altman J. and Das G.D. (1965). Autoradiographic and histological evidence of postnatal hippocampal neurogenesis in rats. *J Comp Neurol*, 124(3):319–335.

Alvarez-Buylla A. and Nottebohm F. (1988). Migration of young neurons in adult avian brain. *Nature*, 335(6188):353–354.

Ambrogini P., Lattanzi D., Ciuffoli S., Agostini D., Bertini L., Stocchi V., Santi S., and Cuppini R. (2004). Morpho-functional characterization of neuronal cells at different stages of maturation in granule cell layer of adult rat dentate gyrus. *Brain Res*, 1017(1-2):21–31.

Bayer S.A. (1985). Neuron production in the hippocampus and olfactory bulb of the adult rat brain: addition or replacement? *Ann N Y Acad Sci*, 457:163–172.

Bechara R.G. and Kelly Á.M. (2013). Exercise improves object recognition memory and induces BDNF expression and cell proliferation in cognitively enriched rats. *Behav Brain Res*, 245:96–100.

Ben Abdallah N.M.B., Slomianka L., Vyssotski A.L., and Lipp H.P. (2010). Early age-related changes in adult hippocampal neurogenesis in C57 mice. *Neurobiol Aging*, 31(1):151–161.

Ben-Ari Y., Cherubini E., Corradetti R., and Gaiarsa J.L. (1989). Giant synaptic potentials in immature rat CA3 hippocampal neurones. *J Physiol*, 416:303–325.

Ben-Ari Y., Khazipov R., Leinekugel X., Caillard O., and Gaiarsa J.L. (1997). $GABA_A$, NMDA and AMPA receptors: a developmentally regulated 'ménage à trois'. *Trends Neurosci*, 20(11):523–529.

Ben-Ari Y. (2002). Excitatory actions of GABA during development: the nature of the nurture. *Nat Rev Neurosci*, 3(9):728–739.

Ben-Ari Y., Gaiarsa J.L., Tyzio R., and Khazipov R. (2007). GABA: a pioneer transmitter that excites immature neurons and generates primitive oscillations. *Physiol Rev*, 87(4):1215–1284.

Bergami M., Masserdotti G., Temprana S.G., Motori E., Eriksson T.M., Göbel J., Yang S.M., Conzelmann K.K., Schinder A.F., Götz M., and Berninger B. (2015). A critical period for experience-dependent remodeling of adult-born neuron connectivity. *Neuron*, 85:1–8.

Bergmann O., Liebl J., Bernard S., Alkass K., Yeung M.S.Y., Steier P., Kutschera W., Johnson L., Landén M., Druid H., Spalding K.L., and Frisén J. (2012). The age of olfactory bulb neurons in humans. *Neuron*, 74(4):634–639.

Biebl M., Cooper C.M., Winkler J., and Kuhn H.G. (2000). Analysis of neurogenesis and programmed cell death reveals a self-renewing capacity in the adult rat brain. *Neurosci Lett*, 291(1):17–20.

Bischofberger J., Engel D., Li L., Geiger J.R.P., and Jonas P. (2006). Patch-clamp recording from mossy fiber terminals in hippocampal slices. *Nat Protoc*, 1(4):2075–2081.

Bischofberger J. (2007). Young and excitable: new neurons in memory networks. *Nat Neurosci*, 10(3):273–275.

Bizon J.L. and Gallagher M. (2003). Production of new cells in the rat dentate gyrus over the lifespan: relation to cognitive decline. *Eur J Neurosci*, 18(1):215–219.

Bonaguidi M.A., Wheeler M.A., Shapiro J.S., Stadel R.P., Sun G.J., Ming G.L., and Song H. (2011). In vivo clonal analysis reveals self-renewing and multipotent adult neural stem cell characteristics. *Cell*, 145(7):1142–1155.

Boss B.D., Peterson G.M., and Cowan W.M. (1985). On the number of neurons in the dentate gyrus of the rat. *Brain Res*, 338(1):144–150.

Brown J.P., Couillard-Després S., Cooper-Kuhn C.M., Winkler J., Aigner L., and Kuhn H.G. (2003). Transient expression of doublecortin during adult neurogenesis. *J Comp Neurol*, 467(1):1–10.

Brunner J., Neubrandt M., Van-Weert S., Andrási T., Kleine-Borgmann F.B., Jessberger S., and Szabadics J. (2014). Adult-born granule cells mature through two functionally distinct states. *eLife*, 3:e03104.

Cameron H.A. and McKay R.D. (2001). Adult neurogenesis produces a large pool of new granule cells in the dentate gyrus. *J Comp Neurol*, 435(4):406–417.

Cameron H.A. and Glover L.R. (2015). Adult neurogenesis: beyond learning and memory. *Annu Rev Psychol*, 66:53–81.

Cancedda L., Fiumelli H., Chen K., and Poo M.M. (2007). Excitatory GABA action is essential for morphological maturation of cortical neurons in vivo. *J Neurosci*, 27(19):5224–5235.

Cellot G. and Cherubini E. (2013). Functional role of ambient GABA in refining neuronal circuits early in postnatal development. *Front Neural Circuits*, 7:136.

Chancey J.H., Adlaf E.W., Sapp M.C., Pugh P.C., Wadiche J.I., and Overstreet-Wadiche L.S. (2013). GABA depolarization is required for experience-dependent synapse unsilencing in adult-born neurons. *J Neurosci*, 33(15):6614–6622.

Chancey J.H., Poulsen D.J., Wadiche J.I., and Overstreet-Wadiche L. (2014). Hilar mossy cells provide the first glutamatergic synapses to adult-born dentate granule cells. *J Neurosci*, 34(6):2349–2354.

Chiang P.H., Wu P.Y., Kuo T.W., Liu Y.C., Chan C.F., Chien T.C., Cheng J.K., Huang Y.Y., Chiu C.D., and Lien C.C. (2012). GABA is depolarizing in hippocampal dentate granule cells of the adolescent and adult rats. *J Neurosci*, 32(1):62–67.

Cooper-Kuhn C.M. and Kuhn H.G. (2002). Is it all DNA repair? Methodological considerations for detecting neurogenesis in the adult brain. *Brain Res Dev Brain Res*, 134(1-2):13–21.

Couillard-Despres S., Winner B., Schaubeck S., Aigner R., VroemenM., Weidner N., Bogdahn U., Winkler J., Kuhn H.G., and Aigner L. (2005). Doublecortin expression levels in adult brain reflect neurogenesis. *Eur J Neurosci*, 21(1):1–14.

Couillard-Despres S., Winner B., Karl C., Lindemann G., Schmid P., Aigner R., Laemke J., Bogdahn U., Winkler J., Bischofberger J., and Aigner L. (2006). Targeted transgene expression in neuronal precursors: watching young neurons in the old brain. *Eur J Neurosci*, 24(6):1535–1545.

Crespo D., Stanfield B.B., and Cowan W.M. (1986). Evidence that late-generated granule cells do not simply replace earlier formed neurons in the rat dentate gyrus. *Exp Brain Res*, 62(3):541–548.

Dayer A.G., Ford A.A., Cleaver K.M., Yassaee M., and Cameron H.A. (2003). Short-term and long-term survival of new neurons in the rat dentate gyrus. *J Comp Neurol*, 460(4):563–572.

Deisseroth K., Singla S., Toda H., Monje M., Palmer T.D., and Malenka R.C. (2004). Excitation-neurogenesis coupling in adult neural stem/progenitor cells. *Neuron*, 42(4):535–552.

Deng W., Aimone J.B., and Gage F.H. (2010). New neurons and new memories: how does adult hippocampal neurogenesis affect learning and memory? *Nat Rev Neurosci*, 11(5):339–350.

Deshpande A., Bergami M., Ghanem A., Conzelmann K.K., Lepier A., Götz M., and Berninger B. (2013). Retrograde monosynaptic tracing reveals the temporal evolution of inputs onto new neurons in the adult dentate gyrus and olfactory bulb. *Proc Natl Acad Sci U S A*, 110(12):E1152–E1161.

Dieni C.V., Nietz A.K., Panichi R., Wadiche J.I., and Overstreet-Wadiche L. (2013). Distinct determinants of sparse activation during granule cell maturation. *J Neurosci*, 33(49):19131–19142.

Doetsch F., Caillé I., Lim D.A., García-Verdugo J.M., and Alvarez-Buylla A. (1999). Subventricular zone astrocytes are neural stem cells in the adult mammalian brain. *Cell*, 97(6):703–716.

Drew L.J., Fusi S., and Hen R. (2013). Adult neurogenesis in the mammalian hippocampus: why the dentate gyrus? *Learn Mem*, 20(12):710–729.

Ebihara S., Shirato K., Harata N., and Akaike N. (1995). Gramicidin-perforated patch recording: GABA response in mammalian neurones with intact intracellular chloride. *J Physiol*, 484 (Pt 1):77–86.

Eisch A.J., Barrot M., Schad C.A., Self D.W., and Nestler E.J. (2000). Opiates inhibit neurogenesis in the adult rat hippocampus. *Proc Natl Acad Sci U S A*, 97(13):7579–7584.

Engert F. and Bonhoeffer T. (1999). Dendritic spine changes associated with hippocampal long-term synaptic plasticity. *Nature*, 399(6731):66–70.

Erickson K.I., Voss M.W., Prakash R.S., Basak C., Szabo A., Chaddock L., Kim J.S., Heo S., Alves H., White S.M., Wojcicki T.R., Mailey E., Vieira V.J., Martin S.A., Pence B.D., Woods J.A., McAuley E., and Kramer A.F. (2011). Exercise training increases size of hippocampus and improves memory. *Proc Natl Acad Sci U S A*, 108(7):3017–3022.

Eriksson P.S., Perfilieva E., Björk-Eriksson T., Alborn A.M., Nordborg C., Peterson D.A., and Gage F.H. (1998). Neurogenesis in the adult human hippocampus. *Nat Med*, 4(11):1313–1317.

Ernst A., Alkass K., Bernard S., Salehpour M., Perl S., Tisdale J., Possnert G., Druid H., and Frisén J. (2014). Neurogenesis in the striatum of the adult human brain. *Cell*, 156(5):1072–1083.

Espósito M.S., Piatti V.C., Laplagne D.A., Morgenstern N.A., Ferrari C.C., Pitossi F.J., and Schinder A.F. (2005). Neuronal differentiation in the adult hippocampus recapitulates embryonic development. *J Neurosci*, 25(44):10074–10086.

Fabel K., Wolf S.A., Ehninger D., Babu H., Leal-Galicia P., and Kempermann G. (2009). Additive effects of physical exercise and environmental enrichment on adult hippocampal neurogenesis in mice. *Front Neurosci*, 3:50.

Filippov V., Kronenberg G., Pivneva T., Reuter K., Steiner B., Wang L.P., Yamaguchi M., Kettenmann H., and Kempermann G. (2003). Subpopulation of nestin-expressing progenitor cells in the adult murine hippocampus shows electrophysiological and morphological characteristics of astrocytes. *Mol Cell Neurosci*, 23(3):373–382.

Francis F., Koulakoff A., Boucher D., Chafey P., Schaar B., Vinet M.C., Friocourt G., McDonnell N., Reiner O., Kahn A., McConnell S.K., Berwald-Netter Y., Denoulet P., and Chelly J. (1999). Doublecortin is a developmentally regulated, microtubule-associated protein expressed in migrating and differentiating neurons. *Neuron*, 23(2):247–256.

Freund T.F. and Buzsáki G. (1996). Interneurons of the hippocampus. *Hippocampus*, 6(4):347–470.

Fuentealba P., Klausberger T., Karayannis T., Suen W.Y., Huck J., Tomioka R., Rockland K., Capogna M., Studer M., Morales M., and Somogyi P. (2010). Expression of COUP-TFII nuclear receptor in restricted GABAergic neuronal populations in the adult rat hippocampus. *J Neurosci*, 30(5):1595–1609.

Fuentealba L.C., Obernier K., and Alvarez-Buylla A. (2012). Adult neural stem cells bridge their niche. *Cell Stem Cell*, 10(6):698–708.

Fukuda S., Kato F., Tozuka Y., Yamaguchi M., Miyamoto Y., and Hisatsune T. (2003). Two distinct subpopulations of nestin-positive cells in adult mouse dentate gyrus. *J Neurosci*, 23(28):9357–9366.

Ganguly K., Schinder A.F., Wong S.T., and Poo M. (2001). GABA itself promotes the developmental switch of neuronal GABAergic responses from excitation to inhibition. *Cell*, 105(4):521–532.

Gao X.B. and van den Pol A.N. (2001). GABA, not glutamate, a primary transmitter driving action potentials in developing hypothalamic neurons. *J Neurophysiol*, 85(1):425–434.

Garaschuk O., Hanse E., and Konnerth A. (1998). Developmental profile and synaptic origin of early network oscillations in the CA1 region of rat neonatal hippocampus. *J Physiol*, 507 (1):219–236.

Garaschuk O., Linn J., Eilers J., and Konnerth A. (2000). Large-scale oscillatory calcium waves in the immature cortex. *Nat Neurosci*, 3(5):452–459.

Ge S., Goh E.L.K., Sailor K.A., Kitabatake Y., Ming G.L., and Song H. (2006). GABA regulates synaptic integration of newly generated neurons in the adult brain. *Nature*, 439(7076):589–593.

Ge S., Pradhan D.A., Ming G.L., and Song H. (2007a). GABA sets the tempo for activity-dependent adult neurogenesis. *Trends Neurosci*, 30(1):1–8.

Ge S., Yang C.H., Hsu K.S., Ming C.L., and Song H. (2007b). A critical period for enhanced synaptic plasticity in newly generated neurons of the adult brain. *Neuron*, 54(4):559–566.

Geiger J.R.P., Bischofberger J., Vida I., Fröbe U., Pfitzinger S., Weber H. J., Haverkampf K., Jonas P. (2002). Patch-clamp recording in brain slices with improved slicer technology. *Pflugers Arch*, 443(3):491-501.

Gleeson J.G., Lin P.T., Flanagan L.A., and Walsh C.A. (1999). Doublecortin is a microtubule-associated protein and is expressed widely by migrating neurons. *Neuron*, 23(2):257–271.

Gould E., Daniels D.C., Cameron H.A., and McEwen B.S. (1992). Expression of adrenal steroid receptors by newly born cells and pyknotic cells in the dentate gyrus of the postnatal rat. *Mol Cell Neurosci*, 3(1):44–48.

Gould E., McEwen B.S., Tanapat P., Galea L.A., and Fuchs E. (1997). Neurogenesis in the dentate gyrus of the adult tree shrew is regulated by psychosocial stress and NMDA receptor activation. *J Neurosci*, 17(7):2492–2498.

Gould E., Reeves A.J., Graziano M.S., and Gross C.G. (1999). Neurogenesis in the neocortex of adult primates. *Science*, 286(5439):548–552.

Grabiec M., Turlejski K., and Djavadian R. (2009). Reduction of the number of new cells reaching olfactory bulbs impairs olfactory perception in the adult opossum. *Acta Neurobiol Exp (Wars)*, 69(2):168–176.

Gu X. and Spitzer N.C. (1995). Distinct aspects of neuronal differentiation encoded by frequency of spontaneous Ca^{2+} transients. *Nature*, 375(6534):784–787.

Gu Y., Arruda-Carvalho M., Wang J., Janoschka S.R., Josselyn S.A., Frankland P.W., and Ge S. (2012). Optical controlling reveals time-dependent roles for adult-born dentate granule cells. *Nat Neurosci*, 15(12):1700–1706.

Gulledge A.T. and Stuart G.J. (2003). Excitatory actions of GABA in the cortex. *Neuron*, 37(2):299–309.

Harman A., Meyer P., and Ahmat A. (2003). Neurogenesis in the hippocampus of an adult marsupial. *Brain Behav Evol*, 62(1):1–12.

Hsiao Y.H., Hung H.C., Chen S.H., and Gean P.W. (2014). Social interaction rescues memory deficit in an animal model of Alzheimer's disease by increasing BDNF-dependent hippocampal neurogenesis. *J Neurosci*, 34(49):16207–16219.

Jafari M., Soerensen J., Bogdanovi R.M., Dimou L., Götz M., and Potschka H. (2012). Long-term genetic fate mapping of adult generated neurons in a mouse temporal lobe epilepsy model. *Neurobiol Dis*, 48(3):454–463.

Jagasia R., Steib K., Englberger E., Herold S., Faus-Kessler T., Saxe M., Gage F.H., Song H., and Lie D.C. (2009). GABA-cAMP response element-binding protein signaling regulates maturation and survival of newly generated neurons in the adult hippocampus. *J Neurosci*, 29(25):7966–7977.

Kaplan M.S. and Hinds J.W. (1977). Neurogenesis in the adult rat: electron microscopic analysis of light radioautographs. *Science*, 197(4308):1092–1094.

Kaplan M.S. (1981). Neurogenesis in the 3-month-old rat visual cortex. *J Comp Neurol*, 195(2):323–338.

Karten Y.J.G., Jones M.A., Jeurling S.I., and Cameron H.A. (2006). GABAergic signaling in young granule cells in the adult rat and mouse dentate gyrus. *Hippocampus*, 16(3):312–320.

Kempermann G., Kuhn H.G., and Gage F.H. (1997). More hippocampal neurons in adult mice living in an enriched environment. *Nature*, 386(6624):493–495.

Kempermann G., Kuhn H.G., and Gage F.H. (1998). Experience-induced neurogenesis in the senescent dentate gyrus. *J Neurosci*, 18(9):3206–3212.

Kempermann G. and Gage F.H. (2002). Genetic influence on phenotypic differentiation in adult hippocampal neurogenesis. *Brain Res Dev Brain Res*, 134(1-2):1–12.

Kempermann G., Gast D., Kronenberg G., Yamaguchi M., and Gage F.H. (2003). Early determination and long-term persistence of adult-generated new neurons in the hippocampus of mice. *Development*, 130(2):391–399.

Kheirbek M.A., Klemenhagen K.C., Sahay A., and Hen R. (2012). Neurogenesis and generalization: a new approach to stratify and treat anxiety disorders. *Nat Neurosci*, 15(12):1613–1620.

Kim J.Y., Liu C.Y., Zhang F., Duan X., Wen Z., Song J., Feighery E., Lu B., Rujescu D., Clair D.S., Christian K., Callicott J.H., Weinberger D.R., Song H., and Ming G.L. (2012). Interplay between DISC1 and GABA signaling regulates neurogenesis in mice and risk for schizophrenia. *Cell*, 148(5):1051–1064.

Klausberger T., Magill P.J., Márton L.F., Roberts J.D.B., Cobden P.M., Buzsáki G., and Somogyi P. (2003). Brain-state- and cell-type-specific firing of hippocampal interneurons in vivo. *Nature*, 421(6925):844–848.

Kobilo T., Liu Q.R., Gandhi K., Mughal M., Shaham Y., and van Praag H. (2011). Running is the neurogenic and neurotrophic stimulus in environmental enrichment. *Learn Mem*, 18(9):605–609.

Konur S. and Ghosh A. (2005). Calcium signaling and the control of dendritic development. *Neuron*, 46(3):401–405.

Kornack D.R. and Rakic P. (1999). Continuation of neurogenesis in the hippocampus of the adult macaque monkey. *Proc Natl Acad Sci U S A*, 96(10):5768–5773.

Kuhn H.G., Dickinson-Anson H., and Gage F.H. (1996). Neurogenesis in the dentate gyrus of the adult rat: age-related decrease of neuronal progenitor proliferation. *J Neurosci*, 16(6):2027–2033.

Kuhn H.G. and Cooper-Kuhn C.M. (2007). Bromodeoxyuridine and the detection of neurogenesis. *Curr Pharm Biotechnol*, 8(3):127–131.

Kumamoto N., Gu Y., Wang J., Janoschka S., Takemaru K.I., Levine J., and Ge S. (2012). A role for primary cilia in glutamatergic synaptic integration of adult-born neurons. *Nat Neurosci*, 15(3):399–405, S1.

Kwon H.B. and Sabatini B.L. (2011). Glutamate induces *de novo* growth of functional spines in developing cortex. *Nature*, 474(7349):100–104.

Laplagne D.A., Espósito S.M., Piatti V.C., Morgenstern N.A., Zhao C., van Praag H., Gage F.H., and Schinder A.F. (2006). Functional convergence of neurons generated in the developing and adult hippocampus. *PLoS Biol*, 4(12):e409.

Lee H., Lee D., Park C.H., Ho W.K., and Lee S,H. (2012). GABA mediates the network activity-dependent facilitation of axonal outgrowth from the newborn granule cells in the early postnatal rat hippocampus. *Eur J Neurosci*, 36(6):2743–2752.

Leinekugel X., Medina I., Khalilov I., Ben-Ari Y., and Khazipov R. (1997). Ca^{2+} oscillations mediated by the synergistic excitatory actions of GABA(A) and NMDA receptors in the neonatal hippocampus. *Neuron*, 18(2):243–255.

Lepski G., Jannes C.E., Nikkhah G., and Bischofberger J. (2013). cAMP promotes the differentiation of neural progenitor cells *in vitro* via modulation of voltage-gated calcium channels. *Front Cell Neurosci*, 7:155.

Leutgeb J.K., Leutgeb S., Moser M.B., and Moser E.I. (2007). Pattern separation in the dentate gyrus and CA3 of the hippocampus. *Science*, 315(5814):961–966.

Liu Y.B., Lio P.A., Pasternak J.F., and Trommer J.F. (1996). Developmental changes in membrane properties and postsynaptic currents of granule cells in rat dentate gyrus. *J Neurophysiol*, 76(2):1074–1088.

Liu M., Pleasure S.J., Collins A.E., Noebels J.L., Naya F.J., Tsai M.J., and Lowenstein D.H. (2000). Loss of BETA2/NeuroD leads to malformation of the dentate gyrus and epilepsy. *Proc Natl Acad Sci USA*, 97(2):865–870.

Lledo P.M., Alonso M., and Grubb M.S. (2006). Adult neurogenesis and functional plasticity in neuronal circuits. *Nat Rev Neurosci*, 7(3):179–193.

LoTurco J.J., Owens D.F., Heath M.J., Davis M.B., and Kriegstein A.R. (1995). GABA and glutamate depolarize cortical progenitor cells and inhibit DNA synthesis. *Neuron*, 15(6):1287–1298.

Lugert S., Basak O., Knuckles P., Haussler U., Fabel K., Götz M., Haas C.A., Kempermann G., Taylor V., and Giachino C. (2010). Quiescent and active hippocampal neural stem cells with distinct morphologies respond selectively to physiological and pathological stimuli and aging. *Cell Stem Cell*, 6(5):445–456.

Magavi S.S., Leavitt B.R., and Macklis J. D. (2000). Induction of neurogenesis in the neocortex of adult mice. *Nature*, 405(6789):951–955.

Magill S.T., Cambronne X.A., Luikart B.W. , Lioy D.T., Leighton B.H., Westbrook G.L., Mandel G., and Goodman R.H. (2010). microRNA-132 regulates dendritic growth and arborization of newborn neurons in the adult hippocampus. *Proc Natl Acad Sci USA*, 107(47):20382–20387.

Maguire E.A., Gadian D.G., Johnsrude I.S., Good C.D., Ashburner J., Frackowiak R.S., and Frith C.D. (2000). Navigation-related structural change in the hippocampi of taxi drivers. *Proc Natl Acad Sci U S A*, 97(8):4398–4403.

Malberg J.E., Eisch A.J., Nestler E.J., and Duman R.S. (2000). Chronic antidepressant treatment increases neurogenesis in adult rat hippocampus. *J Neurosci*, 20(24):9104–9110.

Maletic-Savatic M., Malinow R., and Svoboda K. (1999). Rapid dendritic morphogenesis in CA1 hippocampal dendrites induced by synaptic activity. *Science*, 283(5409):1923–1927.

Markakis E.A. and Gage F.H. (1999). Adult-generated neurons in the dentate gyrus send axonal projections to field CA3 and are surrounded by synaptic vesicles. *J Comp Neurol*, 406(4):449–460.

Markwardt S.J. and Overstreet-Wadiche L. (2008). GABAergic signalling to adult-generated neurons. *J Physiol*, 586(16):3745-3749.

Markwardt S.J., Wadiche J.I., and Overstreet-Wadiche L. (2009). Input-specific GABAergic signaling to newborn neurons in adult dentate gyrus. *J Neurosci*, 29(48):15063-15072.

Markwardt S.J., Dieni C.V., Wadiche J.I., and Overstreet-Wadiche L. (2011). Ivy/neurogliaform interneurons coordinate activity in the neurogenic niche. *Nat Neurosci*, 14(11):1407–1409.

Marlatt M.W., Potter M.C., Lucassen P.J., and van Praag H. (2012). Running throughout middle-age improves memory function, hippocampal neurogenesis, and BDNF levels in female C57Bl/6J mice. *Dev Neurobiol*, 72(6):943–952.

Mathews E.A., Morgenstern N.A., Piatti V.C., Zhao C., Jessberger S., Schinder A.F., and Gage F.H. (2010). A distinctive layering pattern of mouse dentate granule cells is generated by developmental and adult neurogenesis. *J Comp Neurol*, 518(22):4479–4490.

Mirzadeh Z., Merkle F.T., Soriano-Navarro M., Garcia-Verdugo J.M., and Alvarez-Buylla A. (2008). Neural stem cells confer unique pinwheel architecture to the ventricular surface in neurogenic regions of the adult brain. *Cell Stem Cell*, 3(3):265–278.

Miyata T., Maeda T., and Lee J.E. (1999). NeuroD is required for differentiation of the granule cells in the cerebellum and hippocampus. *Genes Dev*, 13(13):1647–1652.

Mongiat L.A., Espósito M. S., Lombardi G., and Schinder A.F. (2009). Reliable activation of immature neurons in the adult hippocampus. *PLoS One*, 4(4):e5320.

Mullen R.J., Buck C.R., and Smith A.M. (1992). NeuN, a neuronal specific nuclear protein in vertebrates. *Development*, 116(1):201–211.

Namba T., Ming G.L., Song H., Waga C., Enomoto A., Kaibuchi K., Kohsaka S., and Uchino S. (2011). NMDA receptor regulates migration of newly generated neurons in the adult hippocampus via Disrupted-In-Schizophrenia 1 (DISC1). *J Neurochem*, 118(1):34–44.

Nardou R, Ferrari D.C., and Ben-Ari Y. (2013). Mechanisms and effects of seizures in the immature brain. *Semin Fetal Neonatal Med*, 18(4):175–184.

Nottebohm F., Kasparian S., and Pandazis C. (1981). Brain space for a learned task. *Brain Res*, 213(1):99–109.

O'Keefe J. and Dostrovsky J. (1971). The hippocampus as a spatial map. Preliminary evidence from unit activity in the freely-moving rat. *Brain Res*, 34(1):171–175.

O'Keefe J. (1976). Place units in the hippocampus of the freely moving rat. *Exp Neurol*, 51(1):78–109.

Overstreet L.S., Hentges S.T., Bumaschny V.F., de Souza F.S.J., Smart J.L., Santangelo A.M., Low M.J., Westbrook G.L., and Rubinstein M. (2004). A transgenic marker for newly born granule cells in dentate gyrus. *J Neurosci*, 24(13):3251–3259.

Overstreet-Wadiche L., Bromberg D.A., Bensen A.L., and Westbrook G.L. (2005). GABAergic signaling to newborn neurons in dentate gyrus. *J Neurophysiol*, 94(6):4528–4532.

Overstreet-Wadiche L.S., Bromberg D.A., Bensen A.L., and Westbrook G.L. (2006). Seizures accelerate functional integration of adult-generated granule cells. *J Neurosci*, 26(15):4095–4103.

Overstreet-Wadiche L.S. and Westbrook G.L. (2006). Functional maturation of adult-generated granule cells. *Hippocampus*, 16(3):208–215.

Owens D.F., Boyce L.H., Davis M.B., and Kriegstein A.R. (1996). Excitatory GABA responses in embryonic and neonatal cortical slices demonstrated by gramicidin perforated-patch recordings and calcium imaging. *J Neurosci*, 16(20):6414–6423.

Owens D.F. and Kriegstein A.R. (2002). Is there more to GABA than synaptic inhibition? *Nat Rev Neurosci*, 3(9):715–727.

Pallotto M. and Deprez F. (2014). Regulation of adult neurogenesis by GABAergic transmission: signaling beyond $GABA_A$-receptors. *Front Cell Neurosci*, 8:166.

Palmer T.D., Willhoite A.R., and Gage F.H. (2000). Vascular niche for adult hippocampal neurogenesis. *J Comp Neurol*, 425(4):479–494.

Parent J.M., Yu T.W., Leibowitz R.T., Geschwind D.H., Sloviter R.S., and Lowenstein D.H. (1997). Dentate granule cell neurogenesis is increased by seizures and contributes to aberrant network reorganization in the adult rat hippocampus. *J Neurosci*, 17(10):3727–3738.

Parent J.M. and Lowenstein D.H. (2002). Seizure-induced neurogenesis: are more new neurons good for an adult brain? *Prog Brain Res*, 135:121–131.

Payne J.A., Rivera C., Voipio J., and Kaila K. (2003). Cation-chloride co-transporters in neuronal communication, development and trauma. *Trends Neurosci*, 26(4):199–206.

Pernía-Andrade A.J. and Jonas P. (2014). Theta-gamma-modulated synaptic currents in hippocampal granule cells *in vivo* define a mechanism for network oscillations. *Neuron*, 81(1):140–152.

Piatti V.C., Davies-Sala M.G., Espósito M.S., Mongiat L.A., Trinchero M.F., and Schinder A.F. (2011). The timing for neuronal maturation in the adult hippocampus is modulated by local network activity. *J Neurosci*, 31(21):7715–7728.

Rao M.S. and Shetty A.K. (2004). Efficacy of doublecortin as a marker to analyse the absolute number and dendritic growth of newly generated neurons in the adult dentate gyrus. *Eur J Neurosci*, 19(2):234–246.

Redmond L., Kashani A.H., and Ghosh A. (2002). Calcium regulation of dendritic growth via CaM Kinase IV and CREB-mediated transcription. *Neuron*, 34(6):999–1010.

Rizzi M., Perego C., Aliprandi M., Richichi C., Ravizza T., Colella D., Velísková J., Moshé S.L., De Simoni M.G., and Vezzani A. (2003). Glia activation and cytokine increase in rat hippocampus by kainic acid-induced status epilepticus during postnatal development. *Neurobiol Dis*, 14(3):494–503.

Schmidt-Hieber C., Jonas P., and Bischofberger J. (2004). Enhanced synaptic plasticity in newly generated granule cells of the adult hippocampus. *Nature*, 429(6988):184–187.

Schmidt-Hieber C., Jonas P., and Bischofberger J. (2007). Subthreshold dendritic signal processing and coincidence detection in dentate gyrus granule cells. *J Neurosci*, 27(31):8430–8441.

Schmidt-Salzmann C., Li L., and Bischofberger J. (2014). Functional properties of extrasynaptic AMPA and NMDA receptors during postnatal hippocampal neurogenesis. *J Physiol*, 592(Pt 1):125–140.

Scoville W.B. and Milner B. (1957). Loss of recent memory after bilateral hippocampal lesions. *J Neuropsychiatry Clin Neurosci*, 12(1):103–113.

Seib D.R.M., Corsini N.S., Ellwanger K., Plaas C., Mateos A., Pitzer C., Niehrs C., Celikel T., and Martin-Villalba A. (2013). Loss of Dickkopf-1 restores neurogenesis in old age and counteracts cognitive decline. *Cell Stem Cell*, 12(2):204–214.

Seki T. and Arai Y. (1995). Age-related production of new granule cells in the adult dentate gyrus. *Neuroreport*, 6(18):2479–2482.

Snyder J.S., Choe J.S., Clifford M.A., Jeurling S.I., Hurley P., Brown A., Kamhi J.F., and Cameron H.A. (2009). Adult-born hippocampal neurons are more numerous, faster maturing, and more involved in behavior in rats than in mice. *J Neurosci*, 29(46):14484–14495.

Soltesz I. , Bourassa J., and Deschênes M. (1993). The behavior of mossy cells of the rat dentate gyrus during theta oscillations in vivo. *Neuroscience*, 57(3):555–564.

Song J., Sun J., Moss J., Wen Z., Sun G.J., Hsu D., Zhong C., Davoudi H., Christian K.M., Toni N., Ming G.L., and Song H. (2013). Parvalbumin interneurons mediate neuronal circuitry-neurogenesis coupling in the adult hippocampus. *Nat Neurosci*, 16(12):1728–1730.

Spalding K.L., Bergmann O., Alkass K., Bernard S., Salehpour M., Huttner H.B., Boström E., Westerlund I., Vial C., Buchholz B.A., Possnert G., Mash D.C., Druid H., and Frisén J. (2013). Dynamics of hippocampal neurogenesis in adult humans. *Cell*, 153(6):1219–1227.

Spampanato J., Sullivan R.K., Turpin F.R., Bartlett P.F., and Sah P. (2012). Properties of doublecortin expressing neurons in the adult mouse dentate gyrus. *PLoS One*, 7(9):e41029.

Spitzer N.C. (2006). Electrical activity in early neuronal development. *Nature*, 444(7120):707–712.

Squire L.R. (2004). Memory systems of the brain: a brief history and current perspective. *Neurobiol Learn Mem*, 82(3):171–177.

Stanfield B.B. and Trice J.E. (1988). Evidence that granule cells generated in the dentate gyrus of adult rats extend axonal projections. *Exp Brain Res*, 72(2):399–406.

Steiner B., Zurborg S., Hörster H., Fabel K., and Kempermann G. (2008). Differential 24h responsiveness of Prox1-expressing precursor cells in adult hippocampal neurogenesis to physical activity, environmental enrichment, and kainic acid-induced seizures. *Neuroscience*, 154(2):521–529.

Stocca G., Schmidt-Hieber C., and Bischofberger J. (2008). Differential dendritic Ca^{2+} signalling in young and mature hippocampal granule cells. *J Physiol*, 586(16):3795–3811.

Strange B.A., Witter M.P., Lein E.S., and Moser E.I. (2014). Functional organization of the hippocampal longitudinal axis. *Nat Rev Neurosci*, 15(10):655–669.

Sultan S., Gebara E., and Toni N. (2013). Doxycycline increases neurogenesis and reduces microglia in the adult hippocampus. *Front Neurosci*, 7:131.

Takahashi T., Nowakowski R. S., and Caviness V.S., Jr. (1992). BrdU as an S-phase marker for quantitative studies of cytokinetic behaviour in the murine cerebral ventricular zone. *J Neurocytol*, 21(3):185–197.

Tandon P., Yang Y., Das K., Holmes G.L., and Stafstrom C.E. (1999). Neuroprotective effects of brain-derived neurotrophic factor in seizures during development. *Neuroscience*, 91(1):293–303.

Tashiro A., Sandler V.M., Toni N., Zhao C., and Gage F.H. (2006). NMDA-receptor-mediated, cell-specific integration of new neurons in adult dentate gyrus. *Nature*, 442(7105):929–933.

Tashiro A., Makino H., and Gage F.H. (2007). Experience-specific functional modification of the dentate gyrus through adult neurogenesis: a critical period during an immature stage. *J Neurosci*, 27(12):3252–3259.

Temprana S.G., Mongiat L.A., Yang S.M., Trinchero M.F., Alvarez D.D., Kropff E., Giacomini D., Beltramone N., Lanuza G.M., and Schinder A.F. (2015). Delayed coupling to feedback inhibition during a critical period for the integration of adult-born granule cells. *Neuron*, 85(1):116–130.

Toni N., Teng E.M., Bushong E.A., Aimone J.B., Zhao C., Consiglio A., van Praag H., Martone M.E., Ellisman M.H, and Gage F.H. (2007). Synapse formation on neurons born in the adult hippocampus. *Nat Neurosci*, 10(6):727–734.

Toni N, Laplagne D.A., Zhao C., LombardiG., Ribak C.E., Gage F.H., and Schinder A.F. (2008). Neurons born in the adult dentate gyrus form functional synapses with target cells. *Nat Neurosci*, 11(8):901–907.

Toni N. and Sultan S. (2011). Synapse formation on adult-born hippocampal neurons. *Eur J Neurosci*, 33(6):1062–1068.

Tozuka Y., Fukuda S., Namba T., Seki T., and Hisatsune T. (2005). GABAergic excitation promotes neuronal differentiation in adult hippocampal progenitor cells. *Neuron*, 47(6):803–815.

Tronel S., Fabre A., Charrier V., Oliet S.H.R., Gage F.H., and Abrous D.N. (2010). Spatial learning sculpts the dendritic arbor of adult-born hippocampal neurons. *Proc Natl Acad Sci U S A*, 107(17):7963–7968.

Tsukada M., Prokscha A., Ungewickell E., and Eichele G. (2005). Doublecortin association with actin filaments is regulated by neurabin II. *J Biol Chem*, 280(12):11361–11368.

Tyzio R., Holmes G.L., Ben-Ari Y., and Khazipov R. (2007). Timing of the developmental switch in GABA(A) mediated signaling from excitation to inhibition in CA3 rat hippocampus using gramicidin perforated patch and extracellular recordings. *Epilepsia*, 48 Suppl 5:96–105.

Valeeva G., Abdullin A., Tyzio R., Skorinkin A., Nikolski E., Ben-Ari Y., and Khazipovd R. (2010). Temporal coding at the immature depolarizing GABAergic synapse. *Front Cell Neurosci*, 4:1-12.

van Praag H., Christie B.R., Sejnowski T.J., and Gage F.H. (1999). Running enhances neurogenesis, learning, and long-term potentiation in mice. *Proc Natl Acad Sci U S A*, 96(23):13427–13431.

van Praag H., Schinder A.F., Christie B.R., Toni N., Palmer T.D., and Gage F.H. (2002). Functional neurogenesis in the adult hippocampus. *Nature*, 415(6875):1030–1034.

Varea E., Belles M., Vidueira S., Blasco-Ibáñez J.M., Crespo C., Pastor A.M., and Nacher J. (2011). PSA-NCAM is expressed in immature, but not recently generated, neurons in the adult cat cerebral cortex layer II. *Front Neurosci*, 5:1-9.

Veena J., Rao B.S.S., and Srikumar B.N. (2011). Regulation of adult neurogenesis in the hippocampus by stress, acetylcholine and dopamine. *J Nat Sci Biol Med*, 2(1):26–37.

Vetreno R.P. and Crews F.T. (2015). Binge ethanol exposure during adolescence leads to a persistent loss of neurogenesis in the dorsal and ventral hippocampus that is associated with impaired adult cognitive functioning. *Front Neurosci*, 9:35.

Vivar C., Potter M.C., Choi J., Lee J.Y., Stringer T.P., Callaway E.M., Gage F.H., Suh H., and van Praag H. (2012). Monosynaptic inputs to new neurons in the dentate gyrus. *Nat Commun*, 3:1107.

Vivar C., Potter M.C., and van Praag H. (2013). All about running: synaptic plasticity, growth factors and adult hippocampal neurogenesis. *Curr Top Behav Neurosci*, 15:189–210.

Wang Y.F., Gao X.B., and van den Pol A.N. (2001). Membrane properties underlying patterns of GABA-dependent action potentials in developing mouse hypothalamic neurons. *J Neurophysiol*, 86(3):1252–1265.

Wang L.P., Kempermann G., and Kettenmann H. (2005). A subpopulation of precursor cells in the mouse dentate gyrus receives synaptic GABAergic input. *Mol Cell Neurosci*, 29(2):181–189.

Wang C., Liu F., Liu Y.Y., Zhao C.H., You Y., Wang L., Zhang J., Wei B., Ma T., Zhang Q., Zhang Y., Chen R., Song H., and Yang Z. (2011). Identification and characterization of neuroblasts in the subventricular zone and rostral migratory stream of the adult human brain. *Cell Res*, 21(11):1534–1550.

Wang D.D. and Kriegstein A.R. (2011). Blocking early GABA depolarization with bumetanide results in permanent alterations in cortical circuits and sensorimotor gating deficits. *Cereb Cortex*, 21(3):574–587.

Wang B., Wang Z., Sun L., Yang l., Li H., Cole A.L., Rodriguez-Rivera J., Lu H.C.C., and Zheng H. (2014). The amyloid precursor protein controls adult hippocampal neurogenesis through GABAergic interneurons. *J Neurosci*, 34(40):13314–13325.

West M.J., Slomianka L., and Gundersen H.J. (1991). Unbiased stereological estimation of the total number of neurons in the subdivisions of the rat hippocampus using the optical fractionator. *Anat Rec*, 231(4):482–497.

Wong R.O.L. and Ghosh A. (2002). Activity-dependent regulation of dendritic growth and patterning. *Nat Rev Neurosci*, 3(10):803–812.

Yagita Y., Kitagawa K., Ohtsuki T., Ki T., Miyata T., Okano H., Hori M., and Matsumoto M. (2001). Neurogenesis by progenitor cells in the ischemic adult rat hippocampus. *Stroke*, 32(8):1890–1896.

Ylinen A., Soltész I., Bragin A., Penttonen M., Sik A., and Buzsáki G. (1995). Intracellular correlates of hippocampal theta rhythm in identified pyramidal cells, granule cells, and basket cells. *Hippocampus*, 5(1):78–90.

Young C.C., Stegen M., Bernard R., Müller M., Bischofberger J., Veh R.W., Haas C.A., and Wolfart J. (2009). Upregulation of inward rectifier K^+ (Kir2) channels in dentate gyrus granule cells in temporal lobe epilepsy. *J Physiol*, 587(Pt 17):4213–4233.

Young S.Z., Taylor M.M., Wu S., Ikeda-Matsuo Y., Kubera C., and Bordey A. (2012). NKCC1 knockdown decreases neuron production through GABA(A)-regulated neural progenitor proliferation and delays dendrite development. *J Neurosci*, 32(39):13630–13638.

Zhao C., Teng E.M., Summers R.G., Jr, Ming G.L., and Gage F.H. (2006). Distinct morphological stages of dentate granule neuron maturation in the adult mouse hippocampus. *J Neurosci*, 26(1):3–11.

Zhao S., Zhou Y., Gross J., Miao P., Qiu L., Wang D., Chen Q., and Feng G. (2010). Fluorescent labeling of newborn dentate granule cells in GAD67-GFP transgenic mice: a genetic tool for the study of adult neurogenesis. *PLoS One*, 5(9).

7 Nomenclature

ACSF	artificial cerebrospinal fluid
AMPA	α-Amino-3-hydroxy-5-methyl-4-isoxazolepropionic acid
AP	action potential
AP5	D-(-)-2-amino-5-phosphonopentanoic acid, an NMDA-receptor blocker
BDNF	brain-derived neurotrophic factor
BrdU	bromodeoxyuridine
CA3	cornu ammonis area 3
DCX	doublecortin
DMSO	dimethylsulfoxide
DNA	deoxyribonucleic acid
dpi	days post injection
DsRed	Discosoma sp. reef coral red fluorescent protein
E_{GABA}	reversal potential for $GABA_A$ receptor-mediated postsynaptic currents
EPSC	excitatory postsynaptic current
EPSP	excitatory postsynaptic potential
GABA	γ-aminobutyric acid
GC	granule cell
GCL	granule cell layer
GFAP	glial fibrillary acidic protein
GFP/ eGFP	green fluorescent protein/ enhanced green fluorescent protein
GPSC	GABAergic postsynaptic current
GPSP	GABAergic postsynaptic potential
KCC2	K^+-Cl^- extruder, a Cl^- extruder
LTP	long-term potentiation

ML	molecular layer
NBQX	2,3-dioxo-6-nitro-1,2,3,4-tetrahydrobenzo[*f*]quinoxaline-7-sulfonamide, an AMPA-receptor blocker
NKCC1	Na^+-K^+-2Cl^- cotransporter, a Cl^- importer expressed in young neurons
NMDA	N-Methyl-D-aspartic acid
POMC	proopiomelanocortin
PSA-NCAM	polysialylated-neural cell adhesion molecule
R_{in}	input resistance
R_S	series resistance
R_{Seal}	seal resistance
SGZ	subgranular zone
SVZ	subventricular zone
τ_m	membrane time constant
V_{hold}	holding membrane potential
V_{rest}	resting membrane potential
wpi	weeks post injection